Noble metals in polyoxometalates: Structural analysis and catalytic survey
--Manuscript Draft--

Manuscript Number:	
Article Type:	Review Article
Keywords:	Polyoxometalates; Noble metals; Addenda atom; Heteroatom; Heterogeneous catalysis
Corresponding Author:	Masoud Mirzaei Ferdowsi University of Mashhad, Faculty of Science Mashhad, Khorassan Razavi IRAN, ISLAMIC REPUBLIC OF
First Author:	Morteza Tahmasebi
Order of Authors:	Morteza Tahmasebi
	Masoud Mirzaei
	Hossein Eshtiagh-Hosseini
	Antonio Frontera
Abstract:	Noble metals have a significant presence in various structures in polyoxometalate (POM) chemistry. They participate in the POM structures primarily as heteroatoms, i.e., as substituted atoms, instead of as primary addenda atoms. Since the noble metals have good catalytic properties, the importance of synthesizing POM compounds based on these metals and, in particular, investigations into their catalytic activity have increased over the past decade, as brought to light in this review.
Suggested Reviewers:	Ulrich Kortz u.kortz@jacobs-university.de
	Maxim N. Sokolov caesar@niic.nsc.ru
	Anna Proust anna.proust@upmc.fr
	Chika Nozaki Kato sckatou@ipc.shizuoka.ac.jp
	Manuel Aureliano maalves@ualg.pt

Dear Professor B. Lippert

Editor, Inorganica Chimica Acta

I am writing to propose a review-type article for possible publication in Inorganica Chimica Acta on "Noble metals in polyoxometalates: structural analysis and catalytic survey". This manuscript has been written in continuation of our recent strategy concerning to review applications of functional materials, especially in POM chemistry.[1-5]

Since the noble metals have superior catalytic properties, the importance of synthesizing POM compounds based on them is of significant importance to scientific community. This review, is trying to completely cover the noble metal-containing-traditional POM (noble metal as substituted atom or heteroatom), their synthetic methods and their catalytic and photocatalytic properties. Our proposed review features the following structure:

1. **Introduction**
2. **Noble metals as heteroatoms in POMs skeletons**
3. **Noble metals as addenda atom(s) in LPOT (Lacunary polyoxotungstate)**
4. **Conclusions and Perspectives**

I wish to confirm that there is no conflict of interest associated with this manuscript and it has been read and approved by my co-authors. I hope you find this review article suitable for submission to Inorganica Chimica Acta and I look forward to hearing from you soon.

With best wishes from Mashhad,

Masoud Mirzaei

Professor in Inorganic Chemistry

Department of Chemistry,

Faculty of Science,

Ferdowsi University of Mashhad,

Mashhad, Iran

ORCID iD: 0000-0002-7256-4601

Email: mirzaeesh@um.ac.ir

**REVIEW PAPERS PUBLISHED ON POLYOXOMETALATES IN THE LAST FIVE YEARS BY OUR GROUP**

[1] M. Samaniyan, M. Mirzaei, R. Khajavian, H. Eshtiagh-Hosseini and C. Streb, ACS Catal., 2019, 9, 10174-10191.
[2] N. Lotfian, M.M. Heravi, M. Mirzaei, B. Heidari, Appl. Orgenomet. Chem., 2019, 33, e4808.
[3] M. Arefian, M. Mirzaei, H. Eshtiagh-Hosseini and A. Frontera, Dalton Trans., 2017, 46, 6812-6829.
[4] S. Taleghani, M. Mirzaei, H. Eshtiagh-Hosseini and A. Frontera, Coord. Chem. Rev., 2016, 309, 84-106.
[5] M. Mirzaei, H. Eshtiagh-Hosseini, M. Alipour and A. Frontera, Coord. Chem. Rev., 2014, 275, 1-18.
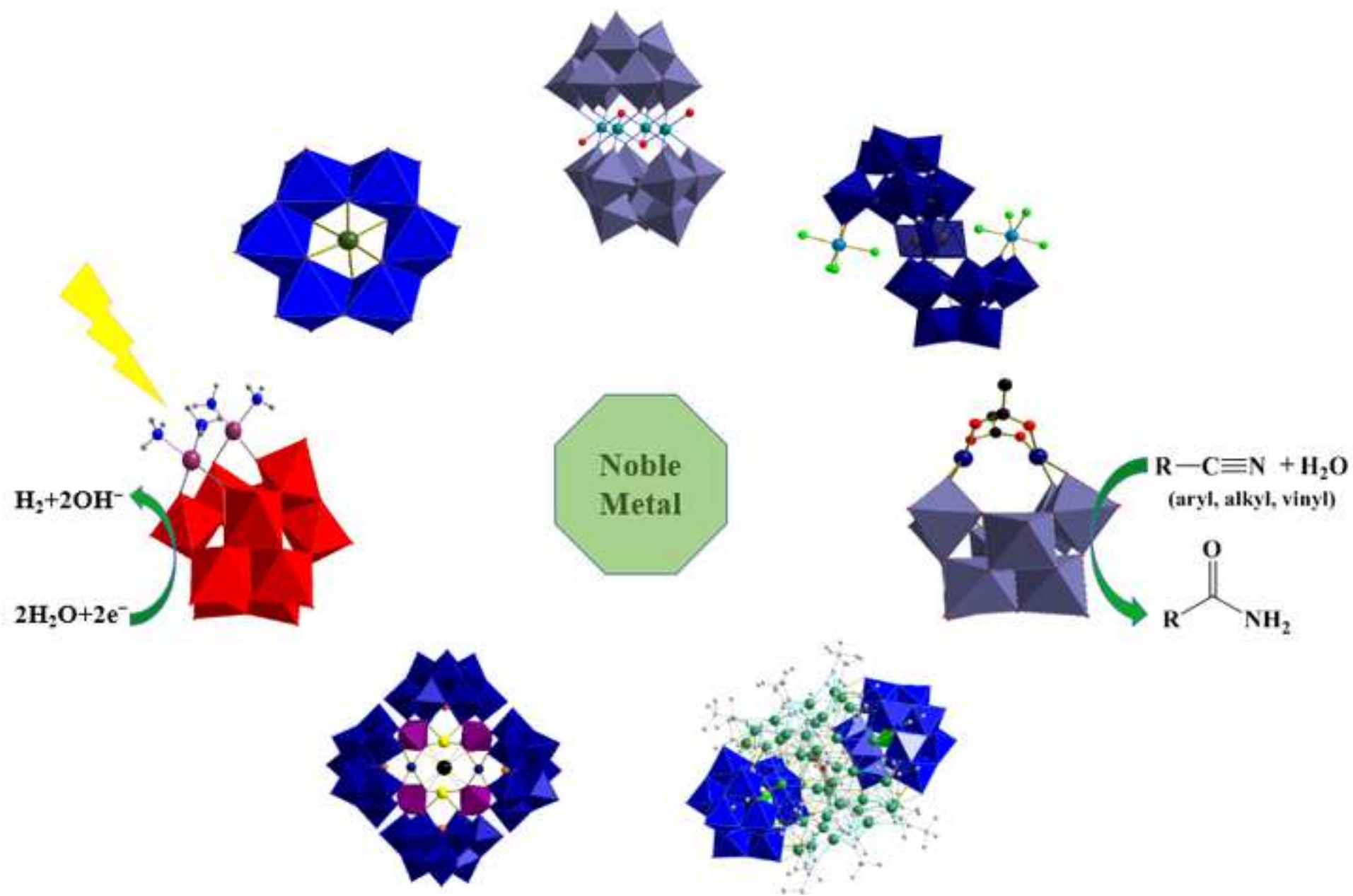
Highlights:

Modifying the polyoxometalates (POMs) to achieve the desired properties has been one of the challenges in this field.

Recently, noble metals, have received more attention due to their prominent catalytic behaviors when incorporated into compounds.

Lacunary POMs can be a good candidate for the formation of noble metal-substituted POMs in order to the modifying POMs.

Noble metals in polyoxometalates: Structural analysis and catalytic survey

Morteza Tahmasebi[a], Masoud Mirzaei[a]*, Hossein Eshtiagh-Hosseini[a] and Antonio Frontera[b]

[a]Department of Chemistry, Faculty of Science, Ferdowsi University of Mashhad, Mashhad 9177948974, Iran

[b]Departament de Química, Universitat de les Illes Balears, Crta. de Valldemossa km 7.5, Palma de Mallorca, Baleares E-07122, Spain

*E-mail: mirzaeesh@um.ac.ir

ABSTRACT

Noble metals have a significant presence in various structures in polyoxometalate (POM) chemistry. They participate in the POM structures primarily as heteroatoms, i.e., as substituted atoms, instead of as primary addenda atoms. Since the noble metals have good catalytic properties, the importance of synthesizing POM compounds based on these metals and, in particular, investigations into their catalytic activity have increased over the past decade, as brought to light in this review.

KEYWORDS

Polyoxometalates; Noble metals; Addenda atom; Heteroatom; Heterogeneous catalysis.

1. Introduction

Given the many energy challenges the world is facing and the importance of achieving clean energy systems, over the last two decades, scientists have made great efforts to prepare chemical compounds that act as successful photocatalysts, thus promoting photocatalytic reactions and the production of H_2 and O_2. Moreover, research into the synthesis of compounds that can act as suitable catalysts to promote various high-yielding organic reactions is also important. Polyoxometalates (POMs) are considered to be excellent candidates in this area of research [1-4]. POMs are a class of transition metal oxide clusters encompassing a large range of structures in terms of size, shape, elemental composition and nuclearity. POMs possess high negative charges, modifiable oxygen-rich surfaces and controllable redox potentials, making them attractive in various research areas, including biology, magnetism, catalysis and material science [5-10]. Indeed, POMs can be subjected to reversible multielectron redox transformations under rather mild conditions without undergoing any significant structural changes, which makes them attractive for catalytic applications. Functionalizing POMs in these materials has always been a challenging and important subject, particularly in terms of retaining the desired properties of the individual components used to construct POM materials [11-15].

In particular, the use of lacunary POMs and the coordination of metal ions as addenda atoms and organometallic fragments into the vacant site(s) of these POMs is one of the most powerful and common techniques for constructing and stabilizing efficient and well-defined metal centers and incorporating precursor properties. Lacunary polyoxotungstate (LPOT), a Wells−Dawson and Keggin−type compound, assumes monovacant and trivacant forms, including $\{XW_{11}O_{39}\}$, $\{X_2W_{17}O_{61}\}$, $\{XW_9O_{33}\}$, $\{XW_9O_{34}\}$, and $\{X_2W_{15}O_{56}\}$, where X = Si, P, As, Ge, and so on, upon the incorporation of metal ions, such as noble ions, and can be used in the formation of metal-substituted monomeric to tetrameric POT clusters [16].

There are eight elements in the second and third series for the transition groups 8-11 (ruthenium (Ru), rhodium (Rh), palladium (Pd), silver (Ag), osmium (Os), iridium (Ir), platinum (Pt), and gold (Au)) that have received attention due to their prominent catalytic behaviors when incorporated into compounds [17-21]. In particular, there has been much research into noble-metal-substituted POM self-assembly. However, noble metals are expensive and rare, limiting their practical applications. Therefore, obtaining the benefits of both POMs and noble metals, as well as overcoming the obstacles of both *via* the substitution of noble metals in vacant spaces in lacunary POMs, is an important research objective in POM chemistry. Lacunary POMs are able to encapsulate almost all of the noble metals, and, in many cases, noble metals enhance their catalytic properties [22-24]. This review covers the POM clusters containing noble elements in various structures and positions and includes the description of the structures of noble metal–containing– traditional POMs (with noble metals as substituted atoms or heteroatoms), the methods used in their syntheses as well as their catalytic and photocatalytic properties.

2. Noble metals as heteroatoms in POMs

Examples of incorporating heteroatoms into the structure of the POMs are mostly of the Anderson–type and, to a lesser extent, Keggin–type POMs. The heteroatoms in heteropolyanion structures have no free coordination sites, and the reactions of such complexes are limited to electron or proton transfer processes. A limited number of metals from the noble metal series, including Ir, Rh, Pt and Pd, have been reported in such structures. An ammonium salt of the Anderson–Evans–type POM anion $[H_6RhMo_6O_{24}]^{3-}$ was prepared in a reaction of $RhCl_3 \cdot 3H_2O$ with $(NH_4)_6[Mo_7O_{24}] \cdot 4H_2O$ at the molar ratio 1:6, and a gallium salt from the same POM anion was obtained when gallium ions was used as a precursor and confirmed *via* crystal structure analysis [25]. For example, a V–

containing Anderson–type heteropolyvanadate $[(C_2H_5)_4N]_4[PdV_6O_{18}]$ was generated *via* the reaction between $[VO_3]^-$ and $[Pd(C_6H_5CN)_2Cl_2]$ precursors. In its structure, four of the six VO_4 units are coordinated to Pd^{II} through an oxygen atom (Fig. 1a) [26]. $[PdMo_6O_{24}H_{3.5}]^{5-}$ is the first example of a heteropolyoxomolybdate–containing palladium(IV) being characterized as a heteroatom *via* X–ray crystallography. In this compound, the two anions share a bridging hydrogen to form a dimer consisting of two $[PdMo_6O_{24}H_3]^{5-}$ monomeric units [27]. Sokolov and colleagues generated $[HIr^{IV}W_6O_{24}]^{7-}$, the first Ir–containing Anderson–Evans type POM anion and the first structurally characterized Ir^{IV}–based POM. The compound was characterized by single–crystal X–ray analysis, IR, UV–Vis, EPR spectroscopies and cyclic voltammetry. *In–situ*–formed Ir^{IV} oxohydroxo complexes and tungstate ions gradually released the $[HIr^{IV}W_6O_{24}]^{7-}$ in solution. The same starting materials use in a rationalized synthetic procedure resulted in the formation of sodium paratungstate $Na_{10}[H_2W_{12}O_{42}] \cdot 25H_2O$ as the main product, whereas a low yield of the $[HIr^{IV}W_6O_{24}]^{7-}$ anion was obtained by the prolonged heating of $K_2[IrF_6]$ with Na_2WO_4 in an aqueous solution at neutral pH. At a higher pH (7.0–7.5), the crystals of non-protonated $[Ir^{IV}W^{VI}O_{24}]^{8-}$ formed as a by–product of $[HIr^{IV}W_6O_{24}]^{7-}$, and, at a pH above 7.6, no crystals were obtained. The $[HIr^{IV}W_6O_{24}]^{7-}$ cluster has an Anderson–Evans–type structure containing six distorted, edge-sharing $W^{VI}O_6$ octahedra that surround a central $Ir^{IV}O_6$ octahedron unit and crystallize in the triclinic space group $P\bar{1}$ (Fig. 1b) [28]. In another report, the reaction between *in–situ*–formed Ir^{IV} oxohydroxo complexes and $Na_9[SbW_9O_{33}]$ in the presence of potassium nitrate resulted in a 28% yield of pale yellow crystals of composition $K_{5.47}Na_{2.3}[Ir_{0.17}Sb_{0.83}W_6O_{24}](NO_3)_{0.6} \cdot 12H_2O$ containing an Anderson–type $[Sb^VW^{VI}_6O_{24}]^{7-}$ POM anion with ~20% of its antimony positions occupied by Ir [29].
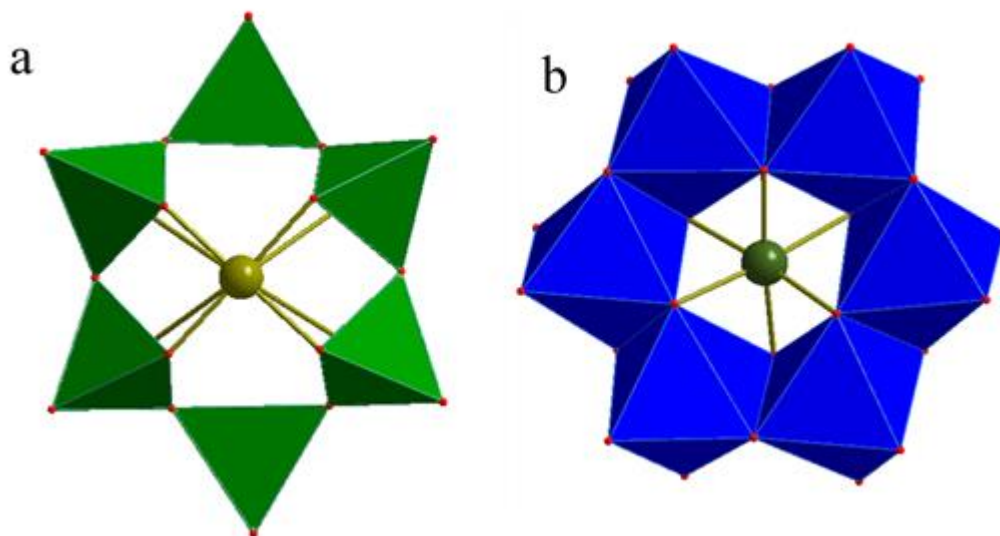
Fig. 1. Structures of (a) $[PdV_6O_{18}]^{4-}$ and (b) $[HIr^{IV}W_6O_{24}]^{7-}$. Color code: $\{VO_4\}$ = green; $\{WO_6\}$ = blue; Pd = dark yellow; Ir = sea green.

3. Noble metals as addenda atom(s) in LPOT

3.1 Ruthenium

Due to the rich and extensive multielectron redox chemistry displayed by ruthenium, reports of the syntheses of ruthenium-containing POMs and their catalytic activities are more abundant than such reports for other noble metals. The Neumann group was the first to report the successful incorporation of ruthenium into the monolacunary $[\alpha\text{-}SiW_{11}O_{39}]^{8-}$, a Keggin–type compound that, together with hydrated $RuCl_3 \cdot nH_2O$, yielded the $[\alpha\text{-}SiW_{11}O_{39}Ru(H_2O)]^{5-}$ POM anion [30]. To synthesize a molybdenum–based, Ru–substituted POM, they used $PMo_{11}O_{39}$ and $RuCl_3 \cdot nH_2O$. The phosphotungstate–type mono–ruthenum-substituted POM anions $[PW_{11}O_{39}Ru^{III}(H_2O)]^{4-}$ was first reported by Pope and Rong, which was obtained *via* the reaction of $[Ru(H_2O)_6]^{2+}$ with $[PW_{11}0_{39}]^{7-}$, followed by oxidation with O_2 [31]. As in the previous cases, the use of $RuCl_3 \cdot nH_2O$ resulted in the formation of a mixed solution. Ligand–bonded ruthenium–water containing the POM anions, $[\alpha\text{-}XW_{11}O_{39}Ru(H_2O)]^{n-}$ (X = Si, P), in most cases, was used as a precursor for the synthesis of similar complexes containing different ligands.

5

$[PW_{11}O_{39}Ru^{II}(H_2O)]^{5-}$ served as a catalyst for water oxidation in the presence of cerium ammonium nitrate as an oxidant, and the results in terms of O_2 evolution were favorable. Between 2006 and 2011, the Sadakane and Kortz groups synthesized and structurally characterized several mono–ruthenium-substituted Keggin–type silicotungstates [30, 32-34]. The reaction of $[SiW_{11}O_{39}]^{8-}$ with Ru(acac)$_3$ under hydrothermal conditions for 20 h yielded $[SiW_{11}O_{39}Ru^{III}(H_2O)]^{5-}$, which had reversible redox couples formed with Ru(V/IV), Ru(IV/III) and Ru(III/II) in an aqueous buffer solution, whereas the prepared complex using RuCl$_3$ was electrochemically inactive [35]. Pyridine derivative Ru–substituted α–Keggin–type silicotungstate was prepared in a reaction of $[\alpha\text{-}SiW_{11}O_{39}Ru(H_2O)]^{5-}$ with pyridine derivatives in water. Single–crystal X–ray analysis proved that the pyridine and its derivatives were coordinated to Ru(III) metals through Ru−N bonds. Here, Ru has a unique redox behavior, as Ru(III) was reversibly oxidized into the Ru(IV) derivative and reduced to the Ru(II) derivative. The structural information concerning most Ru–substituted POMs has been determined by non–X-ray techniques.[30] For $[\{SiW_{11}O_{39}\}Ru^{II}(SO_2)]^{6-}$, another Ru−S–containing POM anion, the electronic structures and features of the bonding between the Ru(II) atom and the SO_2 molecule were investigated *via* DFT and NBO calculations, and the corresponding results were compared with *trans*-$[Ru(NH_3)_4(SO_2)Cl]^+$. The studies indicated that the Ru−S bond in the latter POM anion possesses σ and π bonds and that the bonding interaction between the SO_2 molecule and the Ru^{II} center in $[\{SiW_{11}O_{39}\}Ru^{II}(SO_2)]^{6-}$ is stronger than that in the $[Ru(NH_3)_4Cl]^+$ complex [36]. Deprotonation of the aqua-ruthenium complex $[\alpha\text{–}SiW_{11}O_{39}Ru^{III}(H_2O)]^{5-}$ led to formation of a hydroxy-ruthenium complex $[\alpha\text{–}SiW_{11}O_{39}Ru^{III}(OH)]^{6-}$. Dimerization of two OH-ruthenium complexes led to the formation of the μ–oxo bridged dimer $[\{\alpha\text{-}SiW_{11}O_{39}Ru^{III}\}_2O]^{12-}$ with C_{2v} symmetry and a water molecule (Fig. 2c). As the reaction time for $[SiW_{11}O_{39}]^{8-}$ and Ru(acac)$_3$ increased from 20 h to 5 days, the $[SiW_{11}O_{39}Ru^{III}(H_2O)]^{5-}$ disappeared; eventually, a mixture of light white $[SiW_{12}O_{40}]^{4-}$ powder and black $[\alpha\text{-}SiW_{11}O_{39}Ru^{II}(CO)]$ crystals was generated, in which the black crystals of the carbonyl–ruthenium–substituted POM anion could be

6

separated from the $[SiW_{12}O_{40}]^{4-}$ powder *via* the decantation of the mother liquid. Keggin–type monolacunary phosphotungstate, different salts of ruthenium (or Ru–aqua–containing POM anions) and DMSO have been used as precursors in the preparation of DMSO containing Ru–substituted POM anions [34, 35, 37, 38]. For instance, the reaction of monolacunary $[PW_{11}O_{39}]^{7-}$ with $[Ru^{II}(DMSO)_4]Cl_2$, either under microwave radiation at 200 °C and high pressure, [38] in water at 125 °C under hydrothermal conditions [34] or reacting $[PW_{11}O_{39}]^{7-}$ with $[Ru^{II}(arene)]Cl_2$, followed by light irradiation in the presence of DMSO [37] are convenient synthetic methodologies for obtaining POM anion–containing Ru–DMSO. Moreover, the reaction of the Ru^{II}–aqua derivative, $[PW_{11}O_{39}Ru^{II}(H_2O)]^{5-}$ or $[PW_{11}O_{39}Ru^{III}(H_2O)]^{4-}$ with DMSO in aqueous media leads to the formation of POM–containing Ru–DMSO.[35] Within this family, the ruthenium atom is coordinated to the five oxygen atoms of the lacunary Keggin unit and connected to the DMSO molecule through an Ru–S bond [39, 40]. A NBO calculation for mono–ruthenium phosphotungstate Keggin–type POM anions indicated that the bonding interaction between the Ru(II/III) centers and various ligands comes from the donor–acceptor interaction.[41] The $[SiW_{11}O_{39}Ru^{III}(DMSO)]^{5-}$ POM anion, a non–planar Mo^V–porphyrin complex ($[Mo(DPP)(O)]^+$, DPP^{2-} = dodecaphenylporphyrin) and a mixture containing the two precursors were used as catalysts in the oxidation of benzyl alcohols *via* iodosobenzene in CDCl$_3$ at room temperature to yield the corresponding benzaldehydes. A cyclic voltammetry measurement of the $[SiW_{11}O_{39}Ru^{III}(DMSO)]^{5-}$ POM anion showed two waves at 0.07 and 0.86 V, which were indicative of the Ru$^{III/IV}$ and Ru$^{IV/V}$ couples, respectively. The redox pairs for the Ru$^{III/IV}$ and Ru$^{IV/V}$ couples in the $(TBA)_3\{(Mo(DPP)(O))_2[SiW_{11}O_{39}Ru^{III}(DMSO)]\}$ complex appeared at 0.90 and 1.28 V. Enhancement in catalytic activity of the latter complex, when compared with Ru–POM or porphyrin alone, can be attributed to a large anodic shift in the redox potential of the ruthenium center due to the connection of the cationic $[Mo(DPP)(O)]^+$ unit with the Ru-POM unit.[40] The nitrido ligand is isoelectronic with the oxo ligand, allowing the intercommunity of the N atom in the POM anion structure to act, similar to how the oxo

ligand fulfills in connection to the some transition metals. $[PW_{11}O_{39}N]^{4-}$, the first example of a ruthenium–nitrido derivative of a POM anion, was obtained *via* the direct reaction of $[PW_{11}O_{39}]^{7-}$ with $Cs_2[RuNCl_5]$ or $TBA[RuNCl_4]$. In the latter POM anion, the nitrogen atom can be transferred to PPh_3 derivatives. The reaction of $[PW_{11}O_{39}]^{4-}$ with the PPh_3 mixture yielded the iminophosphorane derivative (n-Bu$_4$N)$_3$ $[PW_{11}O_{39}Ru^V\{NPPh_3\}]$, and, in the presence of (n–Bu$_4$N)OH, a phosphine oxime complex $[PW_{11}O_{39}Ru^{III}\{N(OH)PPh_3\}]^{4-}$ was obtained, which was able to convert to $[PW_{11}O_{39}Ru^{III}\{OPPh_3\}]^{4-}$.[42, 43] The reaction of the dilacunary POM $[\gamma–XW_{10}O_{36}]^{8-}$ (X = Si, Ge) with two equivalents of the metal–nitrido precursor $Cs_2[Ru^{VI}NCl_5]$ formed a dinitridoruthenium–substituted $\gamma–[XW_{10}O_{382}]^{6-}$ (X = Si or Ge) POM anion in each case [44].

In 2013, Sokolov and colleagues reported that a new Ru–containing POM, $[PW_{11}O_{39}Ru^{II}(NO)]^{4-}$, was obtained *via* the reaction of $[Ru(NO)Cl_5]^{2-}$ with $[PW_{11}O_{39}]^{7-}$. The compound was characterized by multinuclear NMR and IR spectroscopies cyclic voltammetry, and electrospray ionization mass spectrometry (ESI-MS). Reactions of $[PW_{11}O_{39}Ru^{II}(NO)]^{4-}$ with both hydrazine and hydroxylamine compounds led to the formation of the aqua complex $[PW_{11}O_{39}Ru^{III}(H_2O)]^{4-}$ in an aqueous solution. Also, the reduction of the nitroso ligand to NH_3 with $SnCl_2$ in water led to the formation of ammonia–coordinated $[PW_{11}O_{39}Ru^{III}(NH_3)]^{4-}$ [45]. Monitoring the reaction of the nitroso complex with hydroxylamine *via* ^{31}P NMR spectroscopy confirmed that an intermediate with coordinated dinitrogen, formulated as $[PW_{11}O_{39}Ru^{II}(N_2)]^{5-}$, was oxidized to the $[PW_{11}O_{39}Ru^{III}(N_2)]^{4-}$ species. A cyclic voltammetry experiment revealed that $[PW_{11}O_{39}Ru^{II}(N_2)]^{5-}$ had a one–electron reversible redox process belonging to the Ru$^{III/II}$ couple. It was difficult to isolate this intermediate from the mixture experimentally, but, in addition to the previously mentioned methods used for detecting the intermediate, theoretical calculations were carried out to study the molecular geometry, electronic structure and metal−dinitrogen bonding nature of the $[PW_{11}O_{39}Ru^{II}(N_2)]^{5-}$intermediate

and some other isostructures formed with other metals, namely, the Os, Re and Ir derivatives [46]. Organometallic transition metal–containing POM anions have received a great deal of attention. The reactions of oxomolybdates, oxotungstates and oxovanadates with aromatic organic compounds, including some derivatives of [{Ru(arene)Cl$_2$}$_2$] (arene = C$_6$H$_6$, C$_6$H$_5$CH$_3$, (η^6-p-MeC$_6$H$_4$$i$Pr), ($\eta^6$-C$_6Me_6$), 1,3,5-C$_6H_3$(CH$_3$)$_3$, 1,2,4,5-C$_6H_2$(CH$_3$)$_4$) in water or organic solvents, led to the formation of the organoruthenium oxomolybdenum, oxotungsten and oxovanadium clusters [47, 48]. In 2006, the Bi and Kortz group synthesized and structurally characterized several clusters of organometallic ruthenium(II) and functionalized heteropolytungstates. [Ru(C$_6$H$_6$)Cl$_2$]$_2$ and dilacunary [γ–MW$_{10}$O$_{36}$] (M = Si, Ge) precursors in water solution yielded a benzene–Ru^{II}–substituted dilacunary decatungstosilicate with the formula [{Ru(C$_6$H$_6$)(H$_2$O)}{Ru(C$_6$H$_6$)}(γ-XW$_{10}$O$_{36}$)]$^{4-}$ (X = Si, Ge). The compound consisted of Ru(C$_6$H$_6$)(H$_2$O) and Ru(C$_6$H$_6$) fragments attached to dilacunary (XW$_{10}$O$_{36}$) Keggin fragments at different sites. The Ru(C$_6$H$_6$)(H$_2$O) group was grafted to the vacant POM anion site *via* two Ru–O(W) bonds and a terminal water molecule and the (RuC$_6$H$_6$) group was grafted to the nonlacunary side *via* three Ru–O(W) bonds to form a cluster with C_s symmetry [49]. The reaction of trilacunary [MW$_9$O$_{34}$]$^{6-}$ (M = Si, Ge) and [RuC$_6$H$_6$Cl$_2$]$_2$ led to the formation of a benzene–Ru(II)–supported trilacunary heteropolytungstate [(RuC$_6$H$_6$)$_2$ MW$_9$O$_{34}$]$^{6-}$ (M = Si, Ge), which was characterized by multinuclear solution NMR and IR spectroscopies, elemental analysis, electrochemical analysis and single–crystal X–ray analysis. The C_s symmetry cluster consisted of two (RuC$_6$H$_6$) fragments. One of the two (RuC$_6$H$_6$) groups was linked to the vacant site of the POM anion through two Ru–O(W) bonds and one Ru–O(X) bond, whereas the second (RuC$_6$H$_6$) group was linked to the non−vacant site *via* three equivalent Ru−O(W) bonds (Fig. 2a) [50].
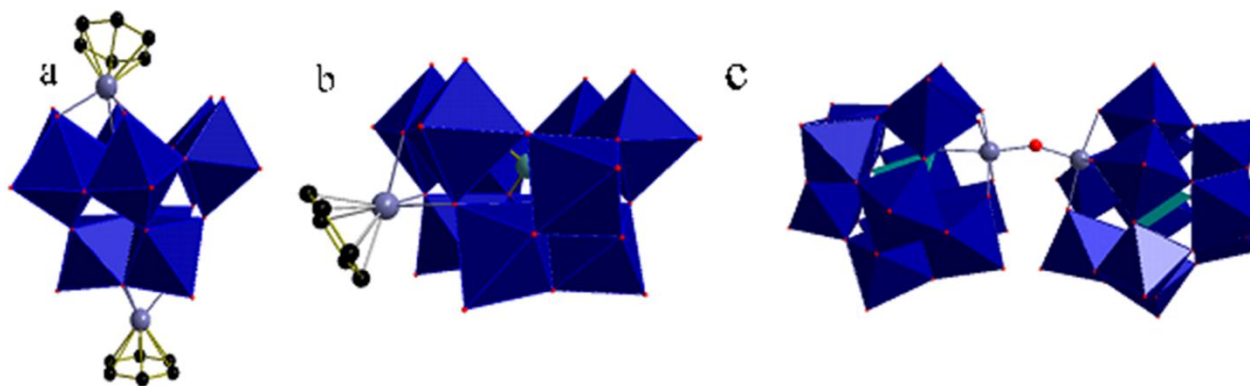
Fig. 2. Structures of (a) $[(RuC_6H_6)_2 MW_9O_{34}]^{6-}$, (b) $[\gamma\text{-}SiW_{10}O_{36}Ru(C_6H_6)]^{6-}$, and (c) $[\{\alpha\text{-}SiW_{11}O_{39}Ru^{III}\}_2O]^{12-}$. Color code: $\{WO_6\}$ = dark blue; $\{SiO_4\}$ = teal; Ru = blue gray; C = black; O = red.

In reports submitted by Bi and colleagues, the reaction of $[(C_{10}H_{14})RuCl_2]_2$ and $[(C_6H_6)RuCl_2]_2$ with $[Sb_2W_{22}O_{74}(OH)_2]^{12-}$ and $[Bi_2W_{22}O_{74}(OH)_2]^{12-}$ led to the formation of $[X_2W_{20}O_{70}(RuC_6H_6)2]^{10-}$ and $[X_2W_{20}O_{70}(RuC_{10}H_{14})_2]^{10-}$ (X = Sb^{III}, Bi^{III}), respectively. The latter POM anions consisted of two lacunary $B–\beta–[XW_9O_{33}]^{9-}$ (X = Sb^{III}, Bi^{III}) Keggin fragments linked *via* two inner *cis*–WO_2 groups and two outer (arene)Ru^{2+} fragments, leading to dimeric structures with idealized C_{2h} symmetry. In other words, each structure can be described as follows: a cluster consisting of a dilacunary $[X_2W_{20}O_{70}]^{14-}$ fragment substituted by two (arene)Ru^{2+} units (similar to what is seen in Fig. 3b). The catalytic activities involving the compounds were carried out *via* the air oxidation of hexadecane and *p*–xylene. The organo ruthenium–containing POM anions had higher yields compared to the all-tungsten derivatives Sb_2W_{22} and Bi_2W_{22} [51]. In another report, released by the same group in 2006, an isostructural compound with a different heteroatom, namely, $[Te_2W_{20}O_{70}(RuC_6H_6)_2]^{8-}$, was obtained *via* the reaction of $[RuC_6H_6Cl_2]_2$ with TeO_2 and $Na_2WO_4·2H_2O$ in an aqueous solution (Fig. 3b). A mono–benzene Ru–substituted dilacunary silicotungstate Keggin–type POM anion, $[\gamma–SiW_{10}O_{36}Ru(C_6H_6)]^{6-}$, was obtained *via* the reaction of $[Ru(C_6H_6)Cl_2]_2$ with $K_8[\gamma–SiW_{10}O_{36}]$. In this case, a cluster consisted of only one $(C_6H_6)Ru^{2+}$ fragment attached

through three non–vacant–site bridging oxygen atoms, resulting in an assembly with an idealized C_s symmetry (Fig. 2b) [52]. Sandwich–type organo–Ru–containing tungstoarsenates with the general formula $[\{B-\alpha-AsW_9O_{33}(OH)\}\{B-\beta-AsW_8O_{30}(OH)\}\{M_4(OH)_2(H_2O)_2\}\{(RuC6H6)3\}]^{6-}$ (M = Ni^{II}, Zn^{II}, Cu^{II}, Mn^{II}, Co^{II}) were obtained *via* the reaction of $[(RuC_6H_6)AsW_9O_{34}]^{7-}$ with the corresponding transitional metal ions. In a departure from previous reports on synthesized organo–Ru–containing POM anions, here, the pre–synthesized organo–Ru functional lacunary species $[(RuC_6H_6)AsW_9O_{34}]^{7-}$ was used as the starting material. Structurally, the POM anions consisted of a rhomb–like (M_4O_{16}) group encapsulated by $[B-\alpha-AsW_9O_{34}]^{9-}$ and $[B\text{-}\beta\text{-}AsW_8O_{31}]^{9-}$ lacunary Keggin fragments, leading to an asymmetric sandwich–type framework material, in which three (RuC_6H_6) units were grafted through Ru−O−W, Ru−O−M and Ru−O−M/W. The catalytic activity involving the compounds was carried out during the oxidation of *n*–hexadecane. The results of the experiments indicated that the catalytic performances of the latter Ru–containing compounds were better than those of similar POM anions without the Ru atom (Fig. 3a) [53].
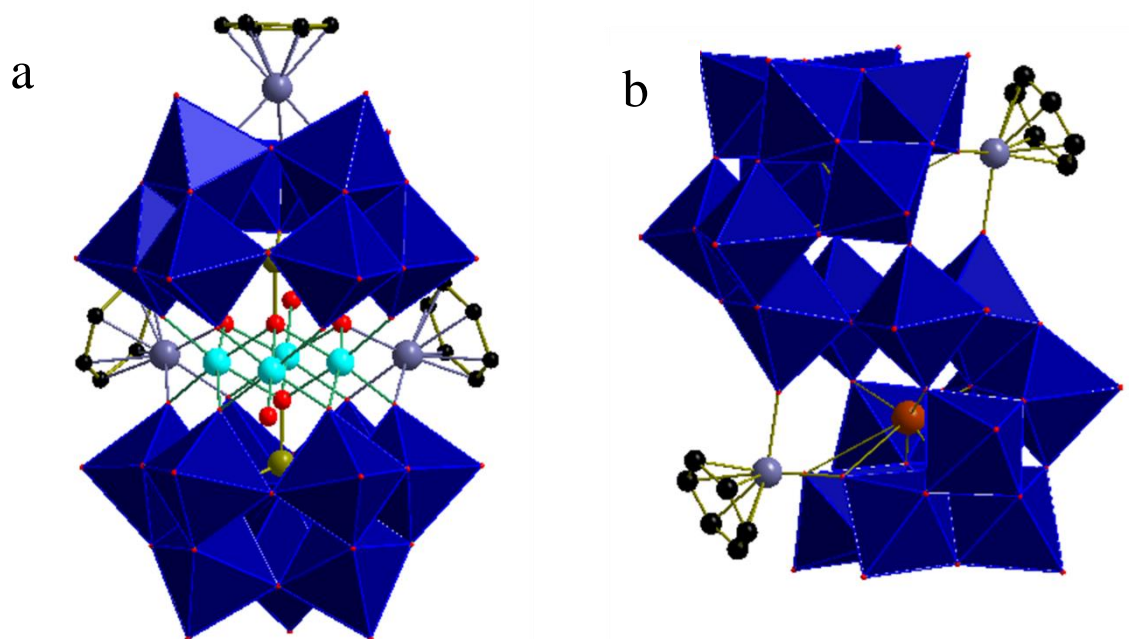
Fig. 3. Structures of (a) [{B-α-AsW$_9$O$_{33}$(OH)}{B-β-AsW$_8$O$_{30}$(OH)}{M$_4$(OH)$_2$(H$_2$O)$_2$}{(RuC$_6$H$_6$)$_3$}]$^{6-}$ and (b) [Te$_2$W$_{20}$O$_{70}$(RuC$_6$H$_6$)$_2$]$^{8-}$. Color code: {WO$_6$} = dark blue; Ru = gray blue; As = dark yellow; Te = brown; Ni = turquoise; C = black; O = red.

[Ru$_4$(μ–O)$_4$(μ–OH)$_2$(H$_2$O)$_4$(γ–SiW$_{10}$O$_{36}$)$_2$]$^{10-}$, briefly Ru$_4$Si$_2$W$_{20}$, the first tetra–ruthenium containing silicotungstate Keggin–type compound, was synthesized and characterized by two groups virtually simultaneously but in different ways [54, 55]. The dilacunary [γ–SiW$_{10}$O$_{36}$]$^{8-}$ POM anion with two equivalents of Ru$_2$OCl$_{10}$$^{4-}$ or RuCl$_3$·H$_2$O in aqueous solution are the main precursors of this remarkable compound. Structurally, the rotation of SiW$_{10}$ fragments by 90° relative to one another gives the compound D_{2d} symmetry. In this compound, the two POM fragments are connected *via* a [Ru$_4$O$_4$(OH)$_2$(H$_2$O)$_4$]$^{6+}$ core. Thus, the two hydroxo groups, each responsible for bridging the two adjacent ruthenium centers attached to the each SiW$_{10}$ unit and oxo ligands, bridge the ruthenium centers of

different monomeric units. The four ruthenium and the six oxygen atoms are at the apexes of a tetrahedron and an octahedron, respectively (Fig. 4a). An isostructure involving the latter cluster, $[Ru^{IV}_4(\mu–O)_2(\mu–OH)_4Cl_4(\gamma–SiW_{10}O_{36})_2]^{12-}$, [56] was obtained *via* the reaction of a dilacunary γ–Keggin silicotungstate $[\gamma–SiW_{10}O_{36}]^{8-}$ with two equivalents of $K_2[RuCl_5(H_2O)]$ (Fig. 4b).
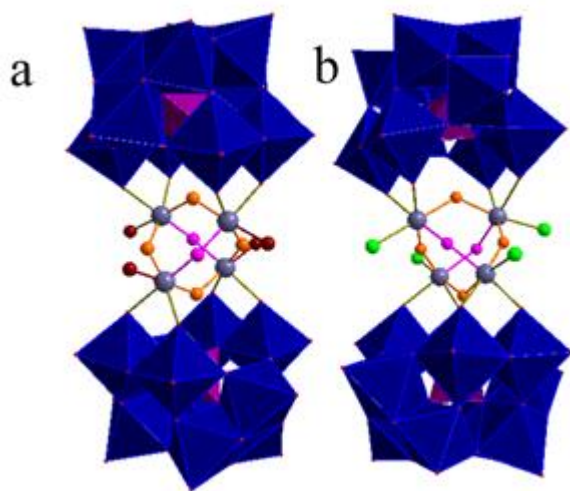
Fig. 4. Structures of (a) $[Ru_4(\mu-O)_4(\mu-OH)_2(H_2O)_4(\gamma-SiW_{10}O_{36})_2]^{10-}$ and (b) $[Ru^{IV}_4(\mu-O)_2(\mu-OH)_4Cl_4(\gamma-SiW_{10}O_{36})_2]^{12-}$. Color code: {WO6} = dark blue; {SiO4} = violet; Ru = blue gray; μ-O = orange; μ-OH = pink; OH2 = dark red; Zn = turquoise.

Sartorel's group evaluated the catalytic ability of $[Ru_4(\mu–O)_4(\mu–OH)_2(H_2O)_4(\gamma–SiW_{10}O_{36})_2]$ in the oxidation of water with an excess of Ce^{IV} *via* the continuous monitoring of the pressure variation and were able to confirm the evolution of molecular oxygen in the system. Studies have shown that the compound is an active and efficient catalyst in the oxidation of water under acidic conditions; the turnover frequency (TOF) was shown to be 450 H per hour, and there was a 90% yield with respect to the amount of oxidant [54]. Hill's group used $[Ru(bpy)_3]^{3+}$ reduction in the presence of a catalyst and monitored the reduction *via* accumulated $[Ru(bpy)_3]^{2+}$ both spectrophotometrically and O_2 chromatographically (GC with TC detector) to investigate the catalytic activity of the

compound. Studies by this group also confirm that the corresponding compound is a rapid and stable catalyst for H_2O oxidation to O_2 at a pH of 7 (the maximum yield was approximately 75%) [55]. After the first studies of this compound by these two groups, the compound was further studied by these same groups, as well as different groups, under different conditions with the aim of optimizing strategies of incorporating the Ru_4–POM into efficient devices for catalyzing water oxidation and other applications.

Sartorel's group reported a combined investigation for $M_{10}[Ru_4(H_2O)_4(\mu-O)_4(\mu-OH)_2(\gamma-SiW_{10}O_{36})_2]$ (M = Cs, Li). The electrochemical analysis showed a stepwise reversible redox and protonation/deprotonation transformation of the $Ru_4^{(IV,IV,IV,IV)}$ species to $Ru_4^{(V,V,V,V)}$ and $Ru_4^{(III,III,II,II)}$. When the $Ru_4^{(V,V,V,V)}$ species is formed, the nucleophilic
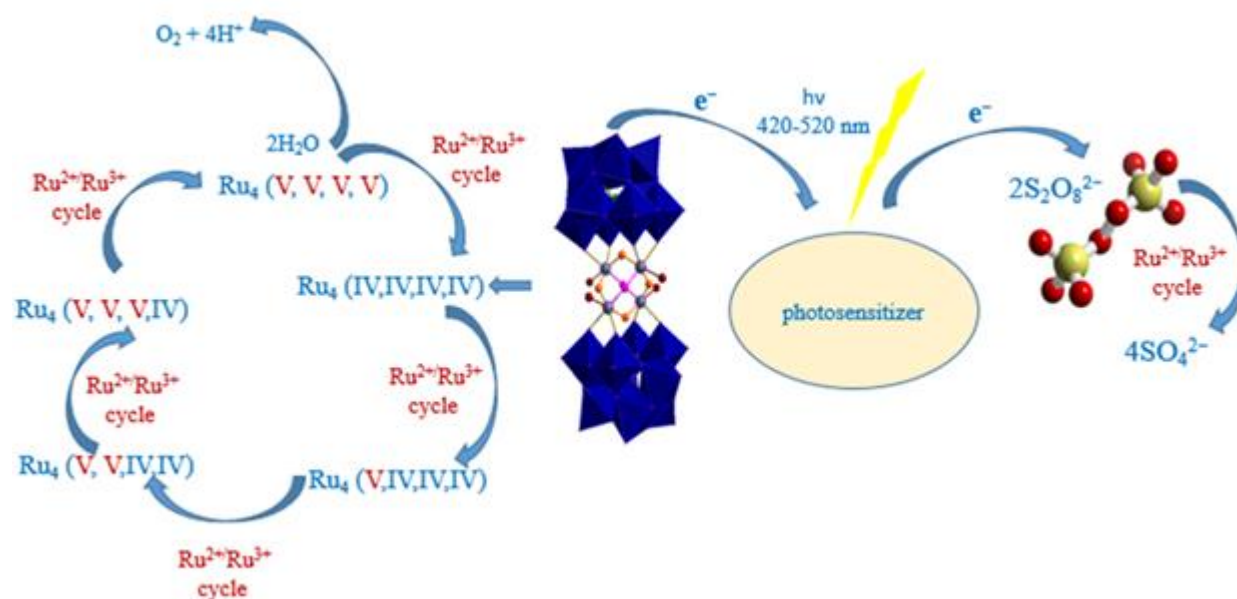
Scheme 1. Photodriven water oxidation *via* $[Ru_4(\mu-O)_4(\mu-OH)_2(H_2O)_4(\gamma-SiW_{10}O_{36})_2]^{10-}$

attack of water on $Ru_4^{(V,V,V,V)}$'s center commences. As a result, a reasonable mode for O–O bond formation. Therefore, the presence of the $Ru_4^{(V,V,V,V)}$ intermediate in this compound makes it an active and efficient catalyst for water oxidation to dioxygen, as in

Scheme 1, [57]. The photocatalytic activity of $[Ru_4(\mu\text{-}O)_4(\mu\text{-}OH)_2(H2O)_4(\gamma\text{-}SiW_{10}O_{36})_2]^{10-}$ in a water oxidation system was studied [58]. With $[Ru(bpy)_3]^{2+}$ as the photosensitizer, $S_2O_8^{2-}$ as the sacrificial electron acceptor, and a tetra–rutenium POM complex as the catalyst, $[Ru(bpy)_3]^{3+}$ was generated from $[Ru(bpy)_3]^{2+}$ via photooxidation. In this study, the overall quantum yield was estimated to be ∼26% [59]. The $Ru_4(\mu\text{-}O)_4(\mu\text{-}OH)_2(H_2O)_4(\gamma\text{-}SiW_{10}O_{36})_2]^{10-}$ complex can easily come into contact with positively charged oxidants due to its high negative charge and low reorganizational energy, which are brought about by the POM ligands that firmly hold and effectively shield the redox active Ru_4 core from the solvent. Therefore, a complex with these properties can act as a hole scavenger in photocatalytic systems in which a photosensitizer is absorbed on a layer of an n-type semiconductor, such as nanocrystalline TiO_2 [60]. Combining $[Ru_4(\mu\text{–}O)_4(\mu\text{–}OH)_2(H_2O)_4(\gamma\text{–}SiW_{10}O_{36})_2]^{10-}$ with $[Ru((\mu\text{–}dpp)Ru(bpy)_2)_3](PF_6)_8$, (bpy = 2,2'–bipyridine; dpp = 2,3–*bis*(2'–pyridyl)pyrazine) as a photosensitizer and $S_2O_8^{2-}$ as a sacrificial oxidant produced photocatalytic activity in the visible–light region in terms of oxygen evolution with a quantum yield of 30% [61]. Photocatalytic oxidation reactions of a cationic water-soluble saddle–distorted porphyrin (H_41^{6+}) with multi–anionic POMs as oxidation catalysts in the photocatalytic oxidation of organic substrates in water under visible–light irradiation were investigated. Among the multi–anionic POMs studied, the assembly $(H_41^{6+})_2$–RuPOM was found to function as an effective photocatalyst for photocatalytic oxidation reactions (PORs) of organic substrates such as benzyl alcohol derivatives [62]. Also, in a similar system, the tri–ruthenium–substituted POM α–$K_6Na[[Ru_3O_3(H_2O)Cl_2](SiW_9O_{34})]\cdot17H_2O$ was used as a hole scavenger. The total turnover number TON (defined as n(O_2)/n(catalyst)) for this compound was lower than those reported for tetra–ruthenium–substituted sandwich–type POM–WOCs; however, the turnover frequency (TOF) was higher than those found in previous results for Ru–POMs [63]. The catalytic activities of $[Ru_4(\mu\text{–}O)_4(\mu\text{–}OH)_2(H_2O)_4(\gamma\text{–}SiW_{10}O_{36})_2]^{10-}$ and a series isostructural POMs of the form $[M_4(\mu\text{-}O)_4(H_2O)_2(PW_9O_{34})_2]^{n-}$ (M = Fe^{III} for n = 6; M = Mn^{II}, Co^{II}, Cu^{II} or Ni^{II} for n = 10) were studied in the presence of H_2O_2, which acted

as the shunt oxidant. The results showed that among these compounds, the tetra-ruthenate catalyst $Ru_4(SiW_{10})_2$ exhibited an unmatched decomposition of H_2O_2 to H_2O and O_2 [64]. A film prepared from $Rb_8K_2[Ru_4(\mu-O)_4(\mu-OH)_2(H_2O)_4(\gamma-SiW_{10}O_{36})_2]\cdot25H_2O$ was used in the reduction of NO_2^-, and the oxidation of ascorbic acid, benzyl alcohol, and dimethyl sulfoxide (DMSO), as well as good bi-functional electrocatalytic activity, was observed. The film also illustrated a good amperometric response to nitrite and ascorbic acid. Therefore, this film is an attractive candidate for an amperometric sensor in the electrocatalytic detection of these two analytes [65]. $Na_{10}[Ru_4(\mu-O)_4(\mu-OH)_2(H_2O)_4(\gamma-SiW_{10}O_{36})_2]$ has been immobilized on glassy carbon electrodes and indium tin oxide (ITO) –coated glass slides *via* the use of a conducting polypyrrole matrix and the layer–by–layer (LBL) technique. The redox behavior and catalytic activity of the prepared film were investigated. Stable redox behavior associated with the Ru centers within the Ru_4POM was observed, and the multilayer assembly displayed a higher oxidation current compared to the POM paste. Therefore, the results demonstrated that Ru_4POM in an LBL assembly with $[RuDend]^{8+}$ has the better performance in the electro-oxidation of water [66]. The catalytic application of immobilized $[Ru_4(\mu-O)_4(\mu-OH)_2(H_2O)_4(\gamma-SiW_{10}O_{36})_2]$ on SBA-15-Apts for the oxidation of n-tetradecane has also been studied. The results indicate that the heterogeneous catalyst $SBA-15-Apts-SiW_{10}Ru_2$ exhibits enhanced catalytic activity compared to naked $[Ru_4(\mu-O)_4(\mu-OH)_2(H_2O)_4(\gamma-SiW_{10}O_{36})_2]$ [67]. By changing the nature of the central heteroatom from Si^{4+} to P^{5+} in the POM−based ligand, the analogue anion based on poorly stable $\gamma-[PW_{10}O_{36}]^{7-}$ was prepared, and its catalytic activity was investigated. Like its silicon analogue, the phosphorus center is capable of catalyzing water oxidation, but the total turnover number TON of $Ru_4P_2W_{20}$ was lower than that for $Ru_4Si_2W_{20}$ in photocatalytic H_2O oxidation due to its slightly lower driving force [68]. In addition to the experimental studies, a number of theoretical studies have also been done to investigate the electronic properties and structural evolution of the tetra-ruthenium catalytic domain [54, 69-71]. In addition to theoretical studies on the tetra–ruthenium transition–metal–substituted POMs, theoretical studies were also performed on single–

Ru–substituted POMs to determine the reaction mechanism involved in the oxidation of H_2O to O_2 when it is catalyzed by this compound [72]. In addition, the electron structures and absorption spectra of a series of transition–metal–substituted POMs, including $SiW_{11}X^{n-}$ (X = Mn^{4+}, Mn^{6+}, Fe^{2+}, Fe^{3+}, Co^{2+}, Ni^{2+}, Ru^{6+}, Re^{6+} and Os^{6+}), was studied *via* DFT and TD–DFT methods to determine whether these compounds could be electron–transfer mediator candidates for DSSCs [73].

Very recently, by Gobbo and colleagues, polymer/nucleotide coacervate microdroplets were reconfigured into membrane-bounded polyoxometalate coacervate vesicles (PCVs) in the presence of the $[Ru_4(\mu\text{-}O)_4(\mu\text{-}OH)_2(H2O)_4(\gamma\text{-}SiW_{10}O_{36})_2]^{10-}$ as a unique catalyst, to produce synzyme protocells (Ru4PCVs) with catalase-like activity [74].

Di–Ru–substituted polyoxotungstate with the formula $Na_{14}[Ru^{III}_2Zn_2(H_2O)_2(ZnW_9O_{34})_2]$ was used to catalyze the electrochemical generation of O_2 using pulsed voltammetry. Cyclic voltammetry showed three waves for this compound pointing to the $Ru^{II/III}$, $Ru^{III/IV}$ and $Ru^{IV/V}$ couples. Therefore, the Ru_2 species can undergo various oxidation states under stepwise, reversible oxidation. Structurally, in this cluster, two (ZnW_9O_{34}) fragments are connected *via* two nickel and two ruthenium centers in the POM anion belt. The two ruthenium centers are bonded to each other directly, and the ruthenium centers bridge the two zinc centers of the central core unit (Fig. 5) [75].
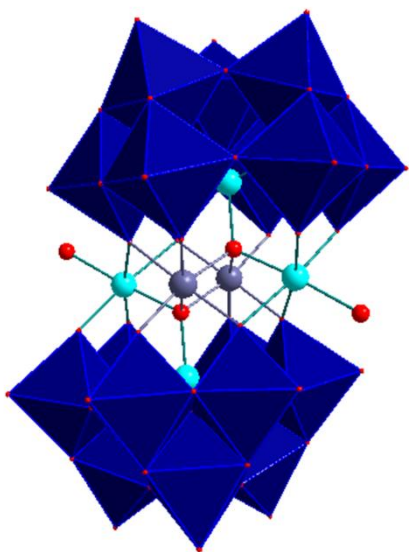
Fig. 5. Structure of $[Ru^{III}_2Zn_2(H_2O)_2(ZnW_9O_{34})_2]^{14-}$. Color code: {WO6} = dark blue; Ru = blue gray; Zn = turquoise.

Reactions of the trilacunary $\alpha-$ and $\beta-$ $[SiW_9O_{34}]^{10-}$ anions with $RuCl_3$ in aqueous solution led to the formation a tetra–ruthenium–substituted $[SiW_9O_{37}Ru_4(H_2O)_3Cl_3]^{7-}$ and, unexpectedly, a tri–ruthenium–containing silicotungstate, $[\{Ru_3O_3(H_2O)Cl_2\}(SiW_9O_{34})]^{7-}$. Attempts to obtain single–crystals of the tetra–ruthenium compound for single–crystal X–ray analysis were unsuccessful. Hence, the determination of the compound's structure was carried out *via* several spectroscopic techniques and magnetic measurements, together with chemical and thermal analyses. However, in the case of the tri–ruthenium cluster, single–crystal X–ray analysis revealed that a trigonal-planar {Ru_3} unit was embedded in the {SiW_9O_{37}} unit and that two Cl atoms and a water molecule coordinated with the {Ru_3} unit. Cyclic voltammetry showed two waves in the positive domain and one wave in the negative domain, which corresponded to the $Ru^{V/IV}$, $Ru^{IV/III}$ and $Ru^{III/II}$ redox processes, respectively. $[\{Ru_3O_3(H_2O)Cl_2\}(SiW_9O_{34})]^{7-}$ was investigated in terms of its performance as a visible–light–driven water oxidation catalyst

(WOC) for O_2 evolution, with $S_2O_8^{2-}$ as a sacrificial electron acceptor and $[Ru(bpy)_3]^{2+}$ as a photosensitizer (PS). POM–PS complexes were formed in the initial phase of the reaction, thus preventing POM decomposition into colloidal oxide catalysts [63].
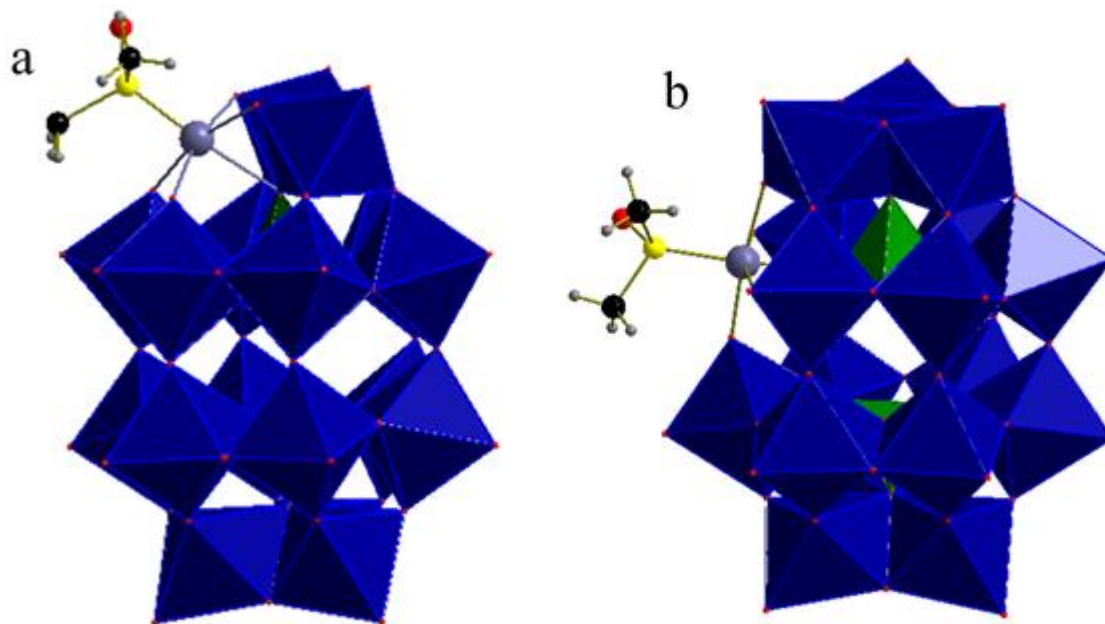

Fig. 6. Structures of (a) $[\alpha_2\text{-}P_2W_{17}O_{61}Ru^{II}(DMSO)]^{8-}$, and (b) $[\alpha_1\text{-}P_2W_{17}O_{61}Ru^{II}(DMSO)]^{8-}$. Color code: $\{WO_6\}$ = dark blue; Ru = blue gray; S = yellow; C = black; O = red.

The number of compounds in which ruthenium is combined with Wells–Dawson–type POMs is still greater than for other metals in this category, with most of them being monomeric and containing a water or DMSO ligand coordinated to the ruthenium center. However, dimer and trimer forms have also been reported for clusters containing ruthenium [76-81]. Mono–Ru–substituted Wells–Dawson type heteropolytungstates with DMSO ligands in the form of both α_1- and α_2-isomers, namely, $[\alpha_1-P_2W_{17}O_{61}Ru^{II}(DMSO)]^{8-}$ and $[\alpha_2-P_2W_{17}O_{61}Ru^{II}(DMSO)]^{8-}$, were obtained *via* the reaction of $[\alpha_2-P_2W_{17}O_{61}]^{10-}$ with $Ru(DMSO)_4Cl_2$ under hydrothermal conditions (Fig. 6a). The main product of this reaction was the α_2-isomer, with $[\alpha_1-$

$P_2W_{17}O_{61}Ru_{II}(DMSO)]^{8-}$ (Fig. 6b), $[PW_{11}O_{39}Ru^{II}(DMSO)]^{5-}$, and $[P_2W_{18}O_{62}]^{6-}$ as by–products. The reaction of $[\alpha_2-P_2W_{17}O_{61}]^{10-}$ with $Ru_2(benzene)_2Cl_4$ led to the production of an isomeric mixture of $[\alpha_1-P_2W_{17}O_{61}Ru^{III}(H_2O)]^{7-}$ and $[\alpha_2-P_2W_{17}O_{61}Ru^{III}(H_2O)]^{7-}$ in which the α_1–isomer was predominant (8 to 1 ratio). Moreover, DMSO–Ru–substituted Wells–Dawson and Keggin–type POMs were also detected as byproducts. In a redox behavior investigation of the $[\alpha_1-P_2W_{17}O_{61}Ru^{II}(DMSO)]^{8-}$ and $[\alpha_2-P_2W_{17}O_{61}Ru^{II}(DMSO)]^{8-}$, cyclic voltammetry showed two waves in the positive domain and two waves in the negative domain. Four well- defined reversible redox pairs ($E_{1/2}$ = 1138, 357, −508, and −743 mV) were observed for the $[\alpha_1-P_2W_{17}O_{61}Ru^{II}(DMSO)]^{8-}$ isomer. The redox pairs at 1138 and 357 mV were attributed to two reversible one-electron transfers for $Ru^{IV/III}(DMSO)$ and $Ru^{III/II}(DMSO)$, and the redox pairs at −508 and −743 mV corresponded to two two–electron reductions of the tungsten. When comparing the redox behaviors of $[\alpha_1-P_2W_{17}O_{61}Ru^{II}(DMSO)]^{8-}$ and $[\alpha_2-P_2W_{17}O_{61}Ru^{II}(DMSO)]^{8-}$ with Ru(DMSO)–substituted α–Keggin–type heteropolytungstates, namely, $[\alpha-XW_{11}O_{39}Ru(DMSO)]^{n-}$ (X = Si, Ge, and P), it is noteworthy that the redox potentials of both the $Ru^{IV/III}$ and $Ru^{III/II}$ processes in DMSO containing Wells–Dawson type POMs were not accompanied by protonation and deprotonation due to these redox processes being independent of the pH, while Keggin–type processes were dependent on the pH value [76].

As the result of the cleavage of the Ru–S bonds in their corresponding DMSO derivatives, $[\alpha_1-P_2W_{17}O_{61}Ru^{II}(DMSO)]^{8-}$ and $[\alpha_2-P_2W_{17}O_{61}Ru^{II}(DMSO)]^{8-}$ produced α_1- and α_2-isomers of mono–Ru–substituted Wells–Dawson type phosphotungstates with aqua ligands, respectively. Mono–Ru–substituted polyoxotungstates with terminal aqua ligands have the ability to replace their water molecules with other ligands, such as pyridine, pyrazine, DMSO, NO, Cl, and CO. In addition, POM complexes containing Ru^V–oxo species are efficient catalysts in terms of the oxidation of water, alcohols, and DMSO. Due to the stronger Ru–H_2O bond conferring a stronger ligand field on the metallic

orbitals, which destabilizes them more than the DMSO ligands can, the WOC activity of an aqua ligand containing Ru–substituted POM anions is higher than those for similar POM anions containing the DMSO ligand [77]. While the latter precursors, *i.e.*, $[\alpha_2-P_2W_{17}O_{61}]^{10-}$ and $Ru(DMSO)_4Cl_2$, led to the formation of monomeric DMSO-Ru-substituted Wells−Dawson type polyoxotungstate under hydrothermal conditions, in another reaction reported by Nomiya and colleagues, the reaction of these same precursors in an ice–cooled, HCl–acidic aqueous solution yielded a dimeric DMSO–Ru–containing polyoxotungstate with the formula $K_{18}[Ru^{II}(DMSO)_2(P_2W_{17}O_{61})_2]\cdot35H_2O$. Due to the poor quality of the resulting crystals, the structure of the POM anion was determined *via* non-crystallographic methods. The techniques used in this experiment suggested that a sandwich dimer structure was formed in which two monovacant Wells–Dawson fragments were connected by a ruthenium center. In the oxidation of the latter dimeric POM anion with Br_2, a monomeric $K_7[\alpha_2-P_2W_{17}O_{61}Ru^{III}(H_2O)]\cdot19H_2O$ was obtained [78]. Another example of a dimeric Wells−Dawson based Ru-containing POM anion is $[O\{Ru^{IV}Cl(\alpha_2-P_2W_{17}O_{61})\}_2]^{16-}$, in which each Ru atom is coordinated by four oxygen atoms of the α_2-Dawson unit, a Cl ligand, and an oxygen bridge between the two $Ru^{IV}Cl(\alpha_2-P_2W_{17}O_{61})$ units [79]. Trimeric ruthenium-substituted isopolyoxotungstate with the formula $Rb_{10}K_3H_6[SeO_3(H_9Ru^{IV}_{5.5}W_{30.5}O_{114})]Cl_3\cdot48H_2O$ (Fig. 7a) was prepared *via* the reaction of $Na_2WO_4\cdot2H_2O$, SeO_2, RbCl and $RuCl_3$ under hydrothermal conditions. The resulting cluster consisted of three monomeric $\{Ru_{1.83}W_{10.17}\}$ units that were condensed to yield a $\{Ru_{5.5}W_{30.5}\}$ unit with a capping $\{SeO_3\}$ pyramidal group. The three $\{Ru_{1.83}W_{10.17}\}$ building blocks were connected to each other through the $\{(Ru/W)O_6\}$ octahedral corners. The selenium center was not incorporated into the structure as a heteroatom. Here it acts as a fragments connector. The electrocatalytic activity of the compound in a nitrite oxidation reaction in an aqueous solution was investigated. The three reversible redox pairs at $E_{1/2}$= +0.93, +0.13, and −0.08 V can be attributed to the Ru^V/Ru^{IV}, Ru^{IV}/Ru^{III}, and Ru^{III}/Ru^{II} redox processes, respectively. In addition, the two well-defined redox waves at $E_{1/2}$ = −0.60 and −1.18 V can be attributed to $W^{VI/V}$ redox

processes in the POM anion. The results of the electrocatalytic studies on the POM anion showed that Ru–containing POM can facilitate the catalysis of the nitrite oxidation reaction, which could possibly benefit from the intrinsically fast electron transfers and redox-activated sites of the Ru centers that are fixed within the cluster set [82].
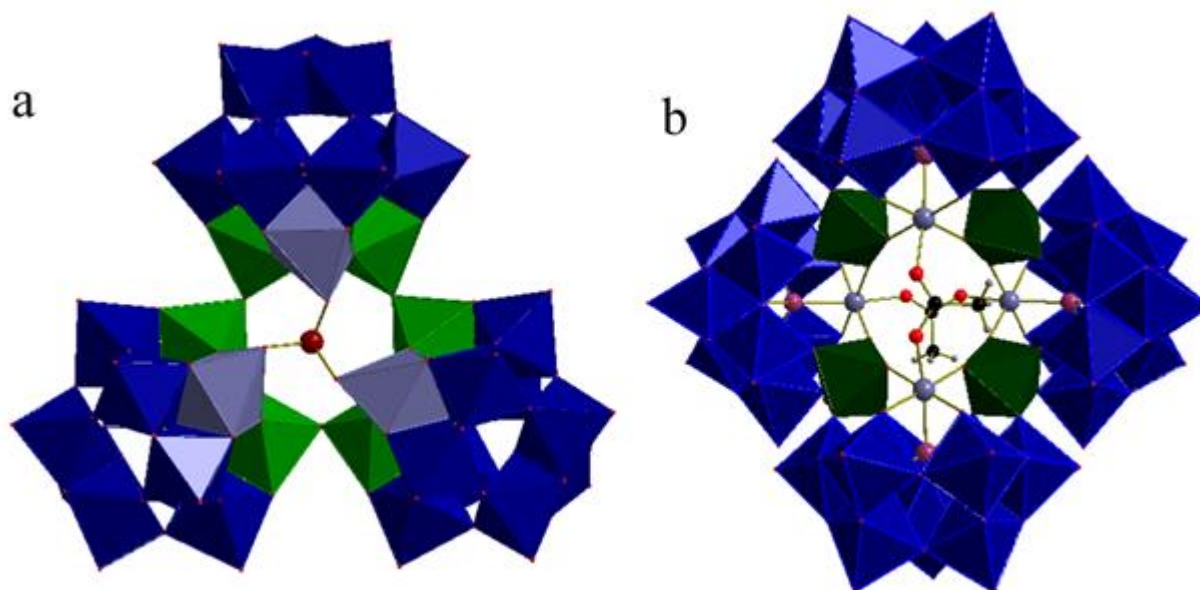

Fig. 7. Structures of (a) $[SeO_3(H_9Ru^{IV}_{5.5}W_{30.5}O_{114})]$, and (b) $[As_4W_{40}O_{140}\{Ru_2(CH_3COO)\}_2]^{14-}$. Color code: $\{WO_6\}$ = dark blue; $\{RuO_6\}$ = green; $\{W/RuO_6\}$ = blue gray; Se = dark red; As = plum; Ru = blue-gray; C = black; O = red.

A crown–shaped acetate-bridged Ru–substituted arsenotungstate with the formula $[H_2N(CH_3)_2]_{14}[As_4W_{40}O_{140}\{Ru_2(CH_3COO)\}_2]\cdot22H_2O$ was obtained *via* the reaction of a mixture of $Na_2WO_4\cdot2H_2O$, $NaAsO_2$, and $RuCl_3$ in the presence of dimethylamine hydrochloride in a sodium acetate buffer solution. The compound consisted of a cyclic unit, namely, $[As_4W_{40}O_{140}]^{28-}$, with two $[Ru_2(CH_3COO)]^{7+}$ fragments embedded in its cavities. The $\{As_4W_{40}\}$ unit was constructed from four trilacunary $[B-\alpha-AsW_9O_{33}]^{9-}$ fragments connected together *via* four additional WO_6 octahedral units (Fig. 7b). The $[As_4W_{40}O_{140}\{Ru_2(CH_3COO)\}_2]$ was investigated in terms of its performance as a catalyst in the heterogeneous oxidation of sulfides with hydrogen peroxide. In this experiment, sulfones in acetonitrile and sulfoxides in methanol were obtained as the selectivity products of the catalytic process. The same oxidation reactions were performed in the

presence of (i) $Na_2WO_4 \cdot 2H_2O$, (ii) $RuCl_3$, and (iii) a mixture of $Na_2WO_4 \cdot 2H_2O$ and $RuCl_3$ as the catalysts. The results indicate a low conversion for the reaction with $RuCl_3$ as the catalyst and a relatively high conversion for the reactions catalyzed by homogeneous (i) $Na_2WO_4 \cdot 2H_2O$ and (ii) a mixture of $Na_2WO_4 \cdot 2H_2O$ and $RuCl_3$. However, these two synthetic materials could not be separated out and reused, while in the case of $[As_4W_{40}O_{140}\{Ru_2(CH_3COO)\}_2]$, the results of recycling experiments implied that there were no obvious changes in the conversion and selectivity of the oxidation of sulfide across several runs [83]. $Cs_3Na_6H[Mo^{VI}_{14}Ru^{IV}_2O_{50}(OH)_2] \cdot 24H_2O$, a wholly inorganic ruthenium-containing polyoxomolybdate, was obtained *via* the reaction of $Na_2Mo^{VI}O_4 \cdot 2H_2O$ and $RuCl_3$ in a solution medium. The compound consisted of a $\{Mo_{14}\}$-type isopolymolybdate unit with a di–ruthenium core embedded in its center. In the presence of tert–butyl hydroperoxide (TBHP) as an oxidant in the reaction medium, the POM anion was used as a heterogeneous catalyst in the oxidation of 1–phenylethanol to acetophenone [84].

3.2 Rhodium

The first Rh^{III}–containing POMs with the formulas $[Rh(PW_{11}O_{39})_2]^{11-}$ and $[Rh(P_2W_{17}O_{61})_2]^{17-}$ were reported in 1979 [85]. These dimeric POM anions were prepared *via* the reaction of lacunary Wells–Dawson and Keggin–type tungstophosphates with $RhCl_3$. In addition, heating divacant $[\gamma–SiW_{10}O_{36}]^{8-}$ with rhodium(II) acetate at 60°C resulted in the formation of $[SiW_{11}O_{39}\{RhCl\}]^{6-}$, which was isolated from mono-Rh-substituted $K_8[SiW_{11}O_{39}\{RhCl\}][Rh_2(CH_3COO)_4C_{l2}] \cdot 8H_2O$, a crystallographically-determined mono-substituted rhodium (Fig. 8) [86].

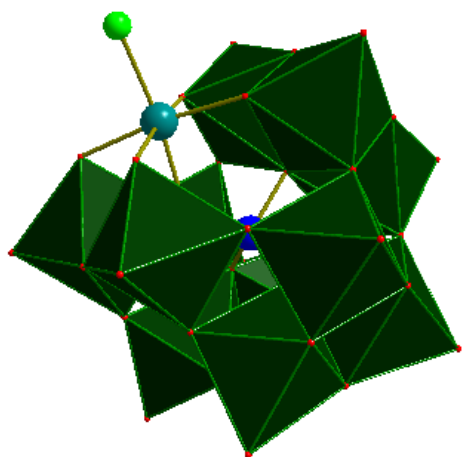**Fig. 8**. Structure of $[SiW_{11}O_{39}\{RhCl\}]^{6-}$. Color code: $\{WO_6\}$ = dark green; Rh = teal; O = red; Si = blue; Cl = green.

Zonnevijlle and colleagues used the monolacunary Wells–Dawson type polyoxotungstate α–$X_2Rh^{III}(OH_2)W_{17}O_{61}]^{7-}$ (X = P, As) and Keggin-type polyoxotungstate to synthesize Rh-substituted POMs in such a manner that Rh was linked to the oxygen atom of the coordinated water molecule [25, 87]. Pope and colleagues synthesized $[(PO_4)W_{11}O_{35}\{Rh_2(OAc)_2\}]^{5-}$, an example of a coordination mode involving a di-rhodium substitution into a lacunary anion in which each rhodium atom is attached to two oxygen atoms of the acetate. This POM anion was synthesized *via* the reaction of a rhodium(II) acetate dimer with lithium 11–tungstophosphate, prepared in situ, at a pH of 3 under hydrothermal conditions [88]. Rhodium-carbon bonds containing $[XW_{11}O_{39}RhCH_2COOH]^{5-,\ 6-}$ (X = P, Si) were obtained *via* a hydrothermal reaction that produced good yields in aqueous solution and involved acetate, $RhCl_3$, and $K_7[PW_{11}O_{39}]$ or $K_8[SiW_{11}O_{39}]$ in an acetate buffer at 120 °C [25]. The CH_2COOH and COOH ligands, both containing Rh-substituted POM anions, were explored in terms of assembling POM-sensitized solar cells (PSSCs). Their photoactivations were studied both before and after

anchoring their POM anions to the TiO$_2$ surface. The results revealed that due to its superior visible–light response, energy level matching, and higher carrier separation efficiency, the COOH ligand with the POM anions displayed a higher photovoltaic response than the [XW$_{11}$O$_{39}$RhCH$_2$COOH]$^{5-}$ one [89]. In the absence of an acetate buffer and in the presence LiCl, the hydrothermal reaction of PW$_{12}$O$_{40}$·xH$_2$O with RhCl$_3$·yH$_2$O led to the formation of [(CH$_3$)$_4$N]$_5$[PW$_{11}$O$_{39}$RhCl]·H$_2$O. To synthesize [(CH$_3$)$_4$N]$_5$[PW$_{11}$O$_{39}$RhBr], a hydrothermal reaction involving the previous reactants, with LiBr substituted LiCl, was carried out in the presence of an acetate buffer. Two byproducts, [PW$_{11}$O$_{39}$RhCl]$^{5-}$ and [PW$_{11}$O$_{39}$Rh(H$_2$O)]$^{4-}$, were isolated from the major product. The reduction of [(CH$_3$)$_4$N]$_5$[PW$_{11}$O$_{39}$RhCl]·H$_2$O in HOAc/NaOAc solution (pH 4.6) on a graphite cloth electrode, followed by the addition of CsCl to the solution, produced the dimeric Rh–Rh bonded species [(PW$_{11}$O$_{39}$Rh)$_2$]$^{10-}$. Oxidation of [(PW$_{11}$O$_{39}$Rh)$_2$]$^{10-}$ *via* air, Br$_2$, or hypochlorite led to the formation of [PW$_{11}$O$_{39}$RhX]$^{4-}$ (X = H$_2$O, Br, Cl, respectively).[10] Pope and colleagues reported another group of di-rhodium-substituted POM anions with diverse organic moieties, namely, [PW$_{11}$O$_{39}${Rh$_2$(O$_2$CR)$_2$}]$^{5-}$ (R = Pr^{n}, CH$_2$Cl, CH$_2$OH, *o*–C$_6$H$_4$OH, *p*–C$_6$H$_4$OH, and [XW$_{11}$O$_{39}${Rh$_2$(pO$_2$CC$_6$H$_4$OH)$_2$}]$^{6-}$; X = Si, Ge), which have been prepared in good yield and characterized by elemental analysis, multinuclear NMR spectroscopy, and the structural crystallography of the cesium salts of the [PW$_{11}$O$_{39}$Rh$_2$(O$_2$CC$_3$H$_7$)$_2$]$^{5-}$ and [PW$_{11}$O$_{39}$Rh$_2$(*p*-O$_2$CC$_6$H$_4$OH)$_2$]$^{5-}$ POM anions [88]. A sandwich-type rhodium polyoxotungstate with an unprecedented tetra–rhodium-oxo core Na$_{12}$[(Rh$_4$(μ_3–O)$_2$(H$_2$O)$_2$)(H$_2$W$_9$O$_{33}$)$_2$]·38H$_2$O was obtained *via* the reaction of Rh$_2$(OAc)$_4$ and sodium tungstate under hydrothermal conditions. In this dimeric POM anion, the polynuclear oxorhodium cluster, in which Rh(II) was oxidized into Rh(III), was placed between trilacunary nonatungstate {W$_9$O$_{33}$} units (Fig. 9) [90].
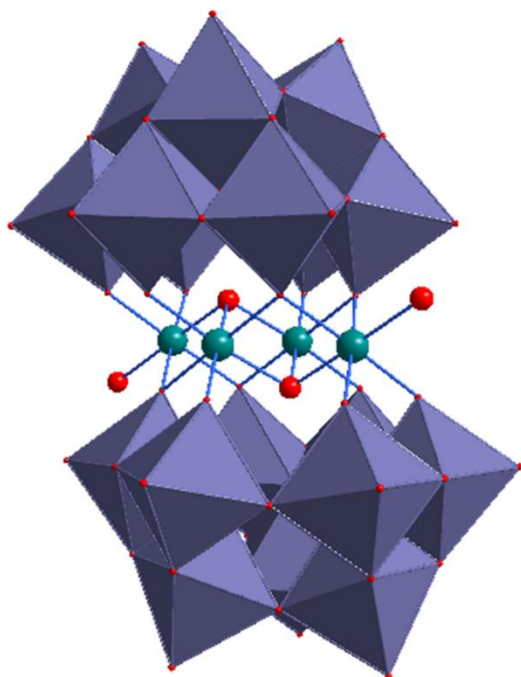
Fig. 9. Structure of $[(Rh_4(\mu_3\text{-}O)_2(H_2O)_2)(H_2W_9O_{33})_2]$. Color code: $\{WO_6\}$ = blue gray; Rh = teal; O = red.

In subsequent attempts to synthesize the new Rh–containing POM anions, Sokolov's group reported the formation of new organometallic derivatives of a POM, namely, $([PW_{11}O_{39}Rh(CH(COOH)_2)])^{5-}$ and $[PW_{11}O_{39}Rh(CH(Ph)COOH)]^{5-}$ *via* reactions of $[PW_{11}O_{39}RhCl]^{5-}$ with malonate and phenyl acetate, respectively. In addition, the separate reactions of $[PW_{11}O_{39}RhCl]^{5-}$ with $RB(OH)_2$ (R = CH_3, Ph (phenyl) and Fc (ferrocenyl)) in aqueous solution under mild heating (40°C) produced $[PW11O39RhCH3]^{5-}$, $[PW_{11}O_{39}RhPh]^{5-}$, and $[PW_{11}O_{39}RhFc]^{5-}$, additional examples of organometallic derivatives of a Rh-substituted Keggin-type polyoxotungstate [91].

The reaction of $(Bu_4N)_5[PW_{11}O_{39}RhCl]$ with NaX (X = NCS^-, N_3^-, and NO_2^-) salts under hydrothermal conditions generated $(Bu_4N)_5[PW_{11}O_{39}Rh(SCN)]$ and $(Bu_4N)_5[PW_{11}O_{39}Rh(NO_2)]$. The reaction of $[PW_{11}O_{39}IrCl]^{5-}$ with NaN_3 led to the formation of an unexpected product: a Keggin-type POM featuring a terminal OH^- ligand.

Electrospray ionization mass-spectrometry (ESI-MS) techniques were used to screen the substitutional reactivities of the {RhCl} groups in $[PW_{11}O_{39}RhCl]^{5-}$ towards alkali salts [92].

Son and colleagues first reported Rh-containing polyoxoniobates $[H_2RhNb_9O_{28}]^{6-}$ and $[Rh_2(OH)_4Nb_{10}O_{30}]^{8-}$, both obtained under hydrothermal reaction conditions. When the temperature was higher, some Rh^{III} was reduced to Rh^0 as a gray or black powder mixed with the crude product. In order to prevent the reduction of Rh^{III}, hydrogen peroxide was added to the reaction mixture. After adding H_2O_2, especially in the case of Rh_2Nb_{10}, the yields improved significantly. Using ESI–MS, it was found that after the hydrothermal reaction, the solution was a mixture of Nb_{10}, Nb_6, $RhNb_9$, and Rh_2Nb_{10} ions. Upon considering the differences in solubility of the compounds, it was concluded that the separation and purification of the Rh-substituted molecules had been accomplished. The structure of the Rh_2Nb_{10} was described as two $RhNb_5$ Lindqvist-type clusters fused by two μ_4–O atoms linking two Rh^{III}. Also, it was determined that Rh^{III} and Nb^V were connected *via* two $\mu3$–O atoms. The oxidation state of rhodium in Rh_2Nb_{10} and $RhNb_9$ was Rh^{III}, as determined *via* a Bond Valence Sum (BVS) calculation [93]. It should be noted that the substitution of Rh into the polyoxoniobates has generally produced low yields.

3.3 Palladium

Recent major advances in the POM chemistry of the palladium atom have been made in the polyoxopalladate field (Pd ions constitute the main addenda atom, which participates in the structure of the POM). However, studies were also conducted in which the palladium was replaced by tungsten or molybdenum in vacant space(s) or in the formation of sandwich-type POM anions [94]. Replacing the palladium atom with the cobalt atom in the polytungstometalate $[WM_3(H_2O)_2(MW_9O_{34})_2]^{12-}$ (M = Zn or Co) gave rise to new Pd, Pt, Ru, and a series of other transitional elements containing POM anions [87]. A few years later, the latter compounds were synthesized again, and their structures and catalytic properties were investigated in depth by the Neumann group. Single–crystal X–ray

analyses of the Ru compound (isostructure with Pd and Pt containing materials) revealed that the structure was compatible with a sandwich-type structure with a WRuZnRu ring between two trilacunary $[B–XW_9O_{34}]^{9-}$ units. The UV and IR spectra of these three compounds proved that they were isostructural compounds. The catalytic activities of these compounds were tested in the oxidation of alkenes and alkanes using aqueous 30% hydrogen peroxide and 70% tert-butyl hydroperoxide as the oxidants, respectively. Also, the catalytic performances of the quaternary ammonium salts of these sandwich–type POMs in the chemoselective, diastereoselective, and regioselective epoxidation of chiral allylic alcohols with H_2O_2 were investigated [95]. Compared to the catalytic activities of the mono-substituted Keggin–type POMs reported previously, the disubstituted sandwich–type POMs were more reactive. Another sandwich–type POMs containing Palladium(II), $K_2Na_6[Pd_2W_{10}O_{36}]\cdot22H_2O$, was obtained via the reaction of an aqueous solution of $Na_2WO_4\cdot 2H_2O$ with K_2PdCl_4. Here, the Pd atoms were heteroatoms in square-planar environments and located between two $W_5O_{18}^{6-}$ groups, which each providing four coordination sites. Various mono-Pd-substituted POM anions were generated via the reactions of Keggin–type polyoxomolybdate and polyoxotungstate $[XW_{11}O_{39}]^{n-}$ (X = B^{III}, Si^{IV}, Ge^{IV}, and P^{V}), and Wells–Dawson type $[\alpha_2\text{-}P_2W_{17}O_{61}]^{10-}$ with $[Pd(H_2O)_4]^{2+}$ or $PdCl_2$ and were characterized by means of UV–Vis, IR as well as ^{17}O, ^{31}P, and ^{183}W NMR spectroscopies [96]. The mono–Pd–substituted POM anions were effective as catalysts in numerous cases, including oxidations of hydrocarbons in $O_2 + H_2$ mixtures, the reduction of hydrogen peroxide, and the hydrogenation of aromatic compounds, compared to ketones.[97, 98] Palladium nanoparticles, which were stabilized by a Keggin−type POM, catalyzed various carbon–carbon and carbon−nitrogen coupling reactions in the reduction of $K_5[PPdW_{11}O_{39}]$ with H_2 [95]. $(Bu_4N)_8[P_2W_{17}Pd(OH_2)O_{61}]$ and some of the transition elements with different oxidation states were tested as chemo− and regioselective oxygen transfer catalysts for H_2O_2 in the epoxidation of allylic alcohols. The reactivity achieved by Pd^{II} –substituted species was higher than those for the other metal-containing species with the same oxidation number evaluated in this experiment [99]. Tri-Pd-containing

complexes $(PW_9)_2Pd_3$ and PW_9Pd_3 were obtained by using $PW_9O_{34}^{9-}$ anion and $Pd(H_2O)_4^{2+}$ as starting materials in a mixture of sulfuric acid and $NaCO_3$ solution. The bimetallics $(PW_9)_2PdFe_2$, $(PW_9)_2Pd_2Fe$, PW_9Pd_2Fe, and $[Pd_2Cu(PW_9O_{34})_2]^{12-}$, plus a mixture of $[Pd_3(PW_9O_{34})_2Pd_nO_xH_y]^{q-}+[(VO)_3(PWO_{34})_2]^{9-}$, were prepared in the presence of $Fe_2(SO_4)_3$ and $CuSO_4$ or $NaVO_3$ under the same conditions. The catalytic performances of the Pd^{II} complexes were tested in terms of the complete reduction of oxygen to water and hydroxylation of benzene to phenol.
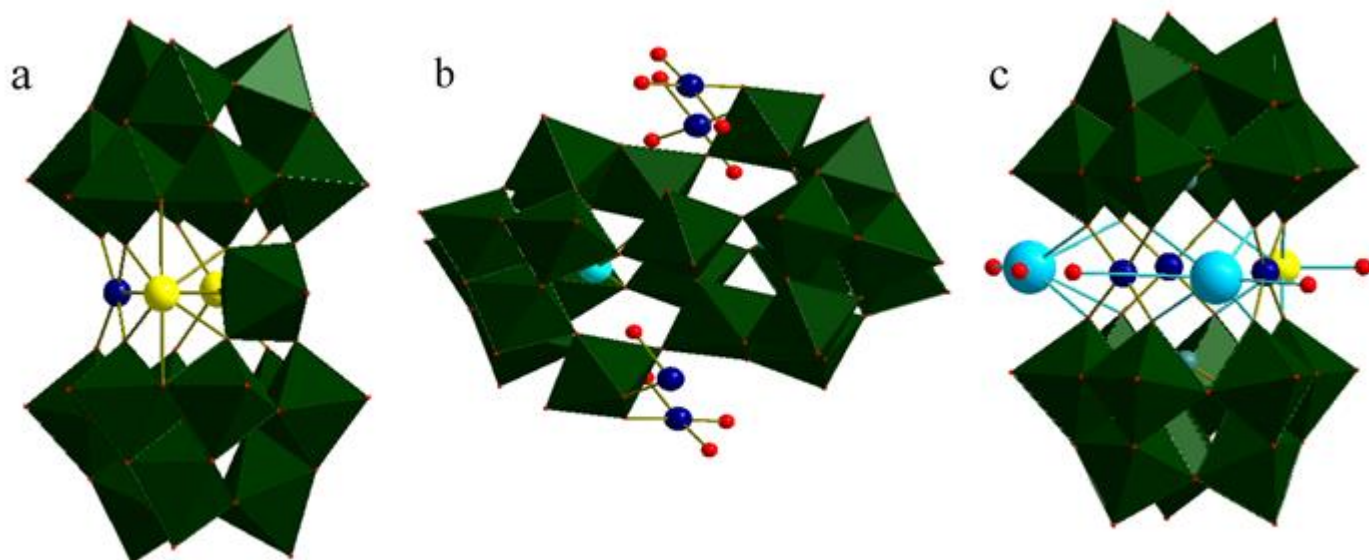

Fig. 10. Structures of (a) $[Na_2(H_2O)_2PdWO(H_2O)(\alpha\text{-}AsW_9O_{33})_2]^{10-}$, (b) $[Pd_3(H_2O)_9Bi_2W_{22}O_{76}]^{8-}$, and (c) $[Cs_2Na(H_2O)_8Pd_3(\alpha\text{-}AsW_9O_{33})_2]^{9-}$. Color code: {WO6} = dark green; Pd = dark blue; Na = yellow; Cs = green; As = turquoise; O = red.

Overall, the results indicate that mono-metallic compounds prepared from trilacunary Keggin–type POMs show poor catalytic activity in the oxidation of hydrocarbons. In contrast, the bimetal Pd^{II}–Fe^{III} complexes with the same anions had active catalytic performances when phenol was produced in the oxidation of benzene and cyclohexane. The bimetallic $[Pd_2Cu(PW_9O_{34})_2]^{12-}$ complex turned out to be inactive in the oxidation [100]. The dilacunary arsenotungstate $[As_2W_{19}O_{67}(H_2O)]^{14-}$ heteropolyanion, in

conjunction with mixing solutions of metal sulfate and $PdSO_4$ in H_2SO_4, was used to form several new bimetallic Pd^{II}, $[As_2W_{19}Pd_2O_{67}(H_2O)_2]^{10-}$, and $M = Fe^{III}$, Ti^{IV}, V^V, Co^{II}, or Cu^{II} complexes. No X–ray structural investigations of any products were obtained, and they were characterized using ^{31}P, [183]W, and [51]V NMR as well as UV–Vis and IR spectroscopies [101]. In 2005, Kortz and colleagues reported the first palladium–substituted tungstoarsenates(III). The mono–Pd^{II}–substituted $[Na_2(H_2O)_2PdWO(H_2O)(\alpha-AsW_9O_{33})_2]^{10-}$ (Fig. 10a) and the tri–Pd^{II}–substituted $[Cs_2Na(H_2O)_8Pd_3(\alpha-AsW_9O_{33})_2]^{9-}$ (Fig. 10c) were synthesized via the reactions of $PdCl_2$ with $[As_2W_{19}O_{67}(H_2O)]^{14-}$ and $[\alpha-AsW_9O_{33}]^{9-}$, respectively, in an aqueous acidic medium and isolated as mixed cesium–sodium salts [102]. A tetramer structure, namely, the palladium-substituted tungstoarsenates POM anion with the formula $K_{17}Na_4[Pd_2Na_2KAs_4W_{40}O_{140}(H_2O)]\cdot63H_2O$ (Fig. 11), was prepared via the reaction of $Na_{28}[As_4W_{40}O_{140}]\cdot60H_2O$ with $PdSO_4$ in a potassium acetate buffer solution, isolated in crystalline form as a hydrated mixed potassium-sodium salt, and characterized by single–crystal X–ray analysis, IR spectroscopy, TGA, and elemental analysis [103].
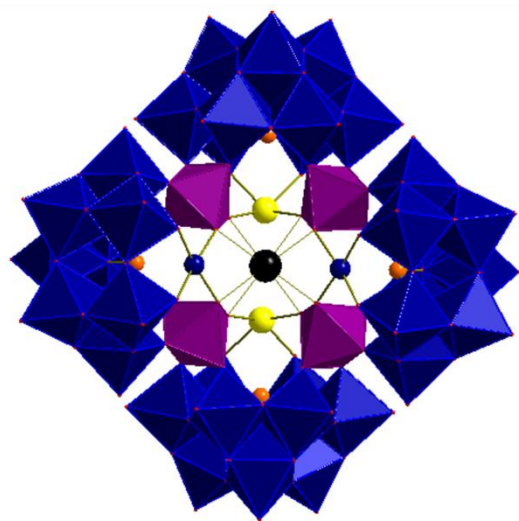

Fig. 11. Structure of $[Pd_2Na_2KAs_4W_{40}O_{140}(H_2O)]^{21-}$. Color code: $\{WO_6\}$ = dark blue/violet; Na = yellow; As = orange; Pd = dark blue; K = black.

Numerous Pd–substituted POMs with various heteroatoms were synthesized by the Lin and Kortz group. In addition to palladium-substituted tungstoarsenates, the pd^{II}– substituted tungstosilicate [Cs$_2$K(H$_2$O)$_7$Pd$_2$WO(H$_2$O)(A-α-SiW$_9$O$_{34}$)$_2$]$^{9-}$ (Fig. 13a), and palladium–substituted tungstoantimonate(III) Cs$_3$KNa$_5$[Cs$_2$Na(H$_2$O)$_{10}$Pd$_3$(SbW$_9$O$_{33}$)$_2$]·16.5H$_2$O were reported. These POM anions were synthesized *via* the reaction of Pd(CH$_3$COO)$_2$ with K$_{10}$[A–α–SiW$_9$O$_{34}$] and Na$_9$[SbW$_9$O$_{33}$] in an aqueous acidic medium. IR spectroscopy, elemental analysis, and electrochemistry, as well as single–crystal X-ray analysis, were used to determine the structures of these POM anions. According to the characterizations, generally, in this series of POM anions, the samples contained two lacunary B–α–[AsW$_9$O$_{33}$]$^{9-}$ Keggin fragments linked by Pd atoms and WO(H$_2$O)$^{4+}$ moieties, leading to sandwich-type structures with C_2v symmetry [102, 104]. Also, a dimeric pd^{II}–substituted tungstobismuthate(III) Na$_5$Pd$_{1.5}$[Pd$_3$(H$_2$O)$_9$Bi$_2$W$_{22}$O$_{76}$]·22H$_2$O (Fig. 10b) was obtained *via* the reaction of PdCl$_2$ with Na$_{12}$[Bi$_2$W$_{22}$O$_{74}$(OH)$_2$] in an aqueous acidic medium. The structure of the latter POM anion is different from the other palladium–containing POMs mentioned thus far, as the palladium metal ion was grafted onto the surface of the POM anion [105].

In a report provided by Hirano and colleagues, the reaction of Pd(OAc)$_2$ and dilacunary [(n–C$_4$H$_9$)$_4$N]$_4$[γ–SiW$_{10}$O$_{34}$(H$_2$O)$_2$] in a mixed solvent of acetone and water generated a di-palladium-substituted γ–Keggin–type silicodecatungstate, [γ–H$_2$SiW$_{10}$O$_{36}$Pd$_2$(OAc)$_2$]$^{4-}$ (Fig. 12), which was different from the sandwich–type POMs reported previously by the Lin and Kortz group. The structure of this monomeric POM anion consisted of two Pd atoms, a lacunary silicotungstate, and two bidentate acetate ligands. Each Pd atom was coordinated to two oxygen atoms of [γ-SiW$_{10}$O$_{36}$]$^{8-}$ and bridged with two bidentate acetate ligands. The catalytic activation of (i) a mixture of Pd(OAc)$_2$, [(n–C$_4$H$_9$)$_4$N]$_4$[γ– SiW$_{10}$O$_{34}$(H$_2$O)$_2$], and (ii) [γ–H$_2$SiW$_{10}$O$_{36}$Pd$_2$(OAc)$_2$]$^{4-}$ was used to hydrate a structurally diverse set of nitriles, including aromatic, aliphatic, heteroaromatic, and double bond-

containing nitriles. The two systems showed high and similar activities. Kinetic, mechanistic, and DFT calculation studies indicated that the di–palladium site plays an important catalytic role in these hydration processes. To enhance the hydration of nitriles, the cooperative activation of nitrile and water with two or more metallic centers has been proposed. Here, the cooperative activation of nitriles and water *via* the di–palladium site formed on a rigid POM−based framework material led to remarkable catalytic activity in terms of the hydration of nitriles, with lacunary $[\gamma–SiW_{10}O_{36}]^{8-}$ acting as an inorganic ligand to the constructed di–palladium active site [106].

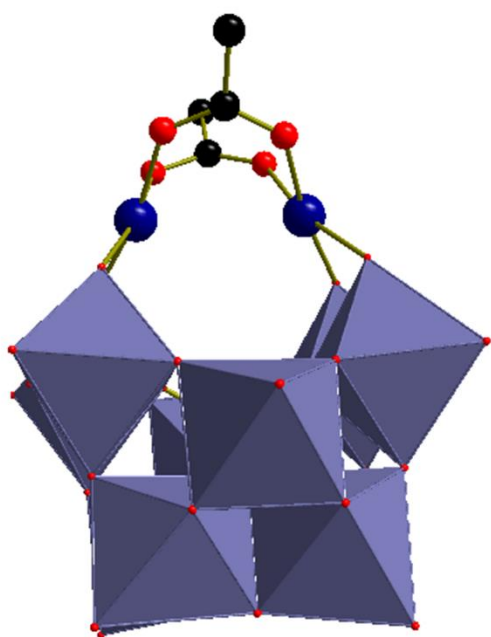**Fig. 12**. Structure of $[\gamma H_2SiW_{10}O_{36}Pd_2(OAc)_2]^{4-}$. Color code: $\{WO_6\}$ = blue gray; Pd = dark blue; C = black; O = red.

Mono-, di-, and tri–Pd–substituted polyoxotungstates, *i.e.*, $K_8[Pd\{WO(H_2O)\}_2\{A,\alpha–PW_9O_{34}\}_2]\cdot20H_2O$, $K_{10}[Pd_2\{WO(H_2O)\}\{A,\alpha–PW_9O_{34}\}_2]\cdot30H_2O$ and $K_{12}[Pd_3\{A,\alpha–PW_9O_{34}\}_2]\cdot30H_2O$, respectively, were obtained *via* the reactions between $[Pd^{II}(NO_3)_2]\cdot H_2O$ and $K_{10}[P_2W_{20}O_{70}(H_2O)_2]\cdot24H_2O$, $K_{12}[P_2W_{19}O_{69}(H_2O)]\cdot24H_2O$, and $K_9[A,\alpha-PW_9O_{34}]\cdot16H_2O$, respectively. The compounds were characterized by IR, ^{31}P and

^{183}W NMR spectroscopies. The $K_{10}[Pd_2\{WO(H_2O)\}\{A,\alpha\text{-}PW_9O_{34}\}_2]\cdot30H_2O$ POM anion (Fig. 13b) was also characterized *via* single–crystal X–ray analysis. Compared to the di–palladium-substituted silicotungstate $[Pd_2\{WO(H_2O)\}\{A,\alpha\text{-}SiW_9O_{34}\}_2]^{12-}$ described by the Kortz and Akari group, which had its counterions located in the central belt of the anion completed by one potassium and two cesium ions, here, the counterions located in this position were completed by three potassium ions [107].
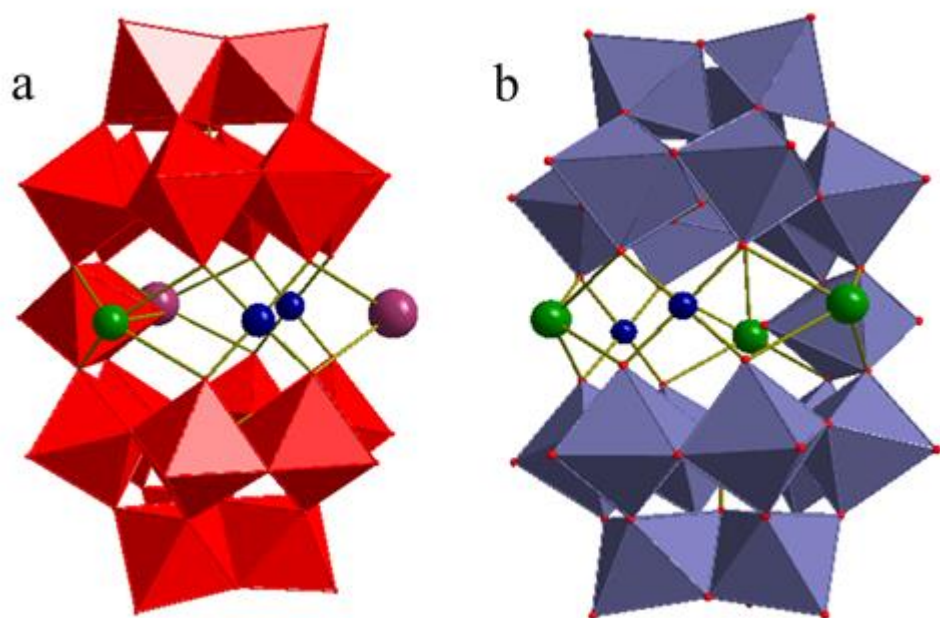

Fig. 13. Structures of (a) $[Pd_2\{WO(H_2O)\}\{A,\alpha\text{-}SiW_9O_{34}\}_2]^{12-}$, and (b) $[Pd_2\{WO(H_2O)\}\{A,\alpha\text{-}PW_9O_{34}\}_2]^{10-}$. Color code: $\{WO_6\}$ = red/blue gray; Pd = dark blue; K = green; Cs = plum.

Another sandwich-type di-palladium-substituted γ–Keggin–type phosphotungstate, $K_9[Pd_2(\alpha\text{-}PW_{11}O_{39}H_{0.5})_2]^{9-}$, with a structure that differed from the structure deduced by Villanneua in 2009, was reported by the Izarova and Kortz group. Here, two lacunary Keggin fragments were linked *via* two Pd^{II} ions in an *anti*-conformation; however, as in

the former compound, the coupling was performed by two palladium ions and $\{WO(H_2O)\}^{4+}$ fragments. The reaction of the Wells–Dawson type POM, $K_{10}[\alpha_2\text{-}P_2W_{17}O_{61}]\cdot17H_2O$, and $PdCl_2$ in solution yielded *anti*– and *syn*–isomers of *di*–palladium-substituted $K_{14}Li[\textit{anti}\text{-}Pd_2(\alpha_2\text{-}P_2W_{17}O_{61}H_{0.5})_2]\cdot50H_2O$. It is noteworthy that here, the reaction of the Pd^{II} ions with monolacunary tungstophosphates did not lead to the incorporation of the Pd^{II} ion into the POM vacancy; instead, it led to the formation of a sandwich–type POM product involving the two Pd atoms [108]. The latter cluster was encapsulated by cetrimonium bromide (CTAB) and tetrabutylammonium bromide (TBAB), respectively, as these surfactants were used to obtain two kinds of assembly structures (nanorolls and hollow spindles) meant to serve as single-atom catalysts (SACs). The assembly structures' catalytic performances in the Suzuki–Miyaura coupling reaction and semi-hydrogenation reaction were then investigated. Although the morphology of the nanorolls changed after the catalytic reaction, FTIR and ^{31}P NMR characterization proved that the structure of the cluster was maintained and that the catalysts could be reused several times without losses in performance [109]. Two trilacunary Wells−Dawson type POM anions incorporated with the Pd^{II} ion in an aqueous medium led to the generation of the sandwich-like tetra–pd^{II}–containing POM $[Pd^{II}_4(\alpha\text{–}P_2W_{15}O_{56})_2]^{16-}$ in *syn*– and *anti*–isomer forms. Due to square-planer Pd^{II} coordination, the Pd_4 unit arrangement in this structure differed from that of other transition metals, since some reported structures have included an adamantane configuration for the Ru_4 core. However, the efficacy of the type of lacunary POM on the configuration of the M_4 part should not be overlooked [110].

The reaction of $Na_{24}[H_6Se_6W_{39}O_{144}]\cdot74H_2O$ and $Pd(NO_3)_2\cdot H_2O$ in various solution media led to the formation of two new selenotungstate/palladate POM anions, namely, $[Se^{IV}_2Pd^{II}_4W^{VI}_{14}O_{56}H]^{11-}$ (Fig. 14a) and $[Se^{IV}_4Pd^{II}_4W^{VI}_{28}O_{108}H_{12}]^{12-}$ (Fig. 14b). In the case of $[Se^{IV}_2Pd^{II}_4W^{VI}_{14}O_{56}H]^{11-}$, the $\{\alpha\text{–}Se_2W_{14}\}$ unit can be compared to a hypothetical tetralacunary Wells–Dawson type $\{\alpha\text{–}P_2W_{14}O_{54}\}$ fragment, and the $\{Pd_4O_4\}$ site in $[Se^{IV}_2Pd^{II}_4W^{VI}_{14}O_{56}H]^{11-}$ can serve an analogy to the vacant site in a lacunary POT. As in

a Wells–Dawson type heteropolyanion, the two central Se^{IV} ions heteroatoms were surrounded by 18 addenda metal ions (here, W_{14} and Pd_4 ions instead of W_{18} ions). $[Se^{IV}_4Pd^{II}_4W^{VI}_{28}O_{108}H_{12}]^{12-}$ can be considered to be a dimer POM anion in which two γ–$\{(H_2O)(OH)_2Pd^{II}_2Se^{IV}_2W_{13}O_{49}\}$ fragments serving as the lacunary derivatives of the hypothetical $\{\alpha\text{-}Pd4Se_2W_{14}\}$ species are connected to each other *via* two *trans-*$\{O=W(H_2O)\}$ groups [111].
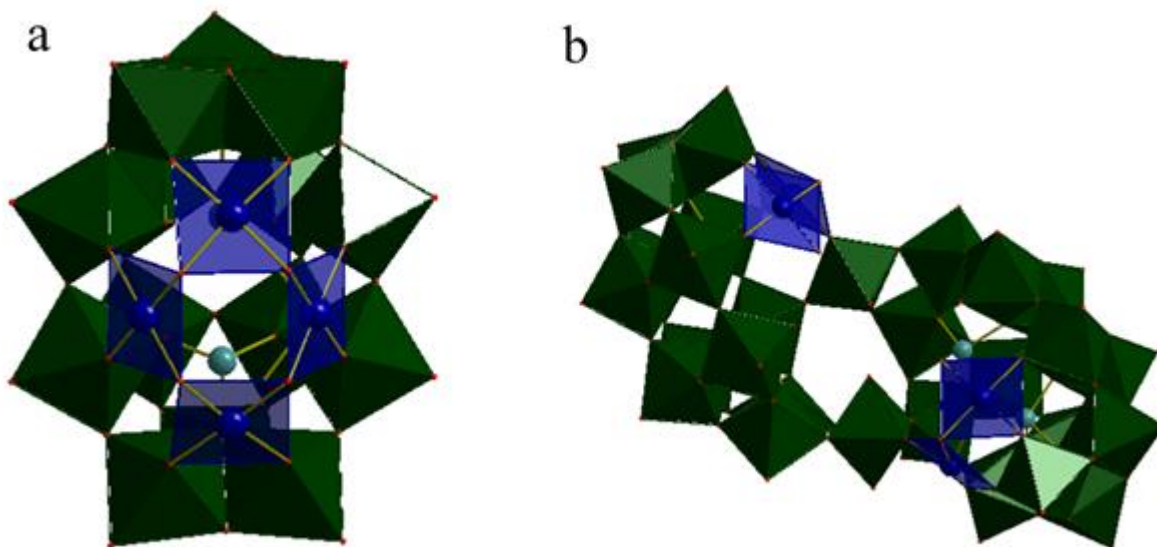
Fig. 14. Structures of (a) $[Se^{IV}_2Pd^{II}_4W^{VI}_{14}O_{56}H]^{11-}$, and (b) $[Se^{IV}_4Pd^{II}_4W^{VI}_{28}O_{108}H_{12}]^{12-}$. Color code: $\{WO6\}$ = dark green; $\{PdO4\}$ = blue; Se = sea green.

3.4 Silver

The first crystallographically–characterized Ag–containing POM was reported by Villanneau and colleagues. It was described as a sandwich–type POM, $[NBu_4]_4[Ag_2\{Mo_5O_{13}(OMe)_4(NO)\}_2]$, consisting of two defective POM anion bridges between two silver cations in slightly distorted square-planar environments (Fig. 15) [112].

Fig. 15. Structure of $[NBu_4]_4[Ag_2\{Mo_5O_{13}(OMe)_4(NO)\}_2]$. Color code: $\{MoO_6\}$ = dark red; Ag = sea green; C = black; N = blue; O = red.

Cases in which silver has been substituted into a polyoxotungstate compound have been reported by various groups. The reaction of monolacunary $[\alpha–PW_{11}O_{39}]^{7-}$ and AgI in an aqueous solution led to the formation of small, needle-s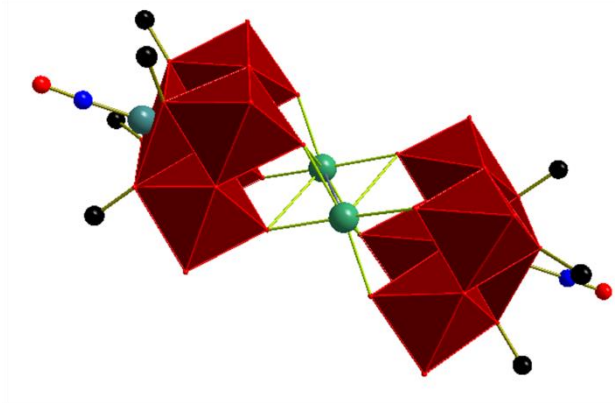haped crystals with the formula $H_2Ag_{0.33}K_{3.67}[AgPW_{11}O_{39}]\cdot 8.25H_2O\cdot CH_3OH$. Ag's metallic center interacts in the solid state with four oxygen atoms from the neighboring $[AgPW_{11}O_{39}]^{6-}$ units to produce a 1D, anionic $[AgPW_{11}O_{39}]_n^{6n-}$ chain.[113] Cui and colleagues synthesized a 1D chain-like Ag^I –substituted Keggin–type polyoxotungstate that is isomorphic with the previous compound. In this case, $K_3[H_3Ag^IPW_{11}O_{39}]\cdot 12H_2O$ was dissolved in an aqueous solution, creating an Ag^I anion–complex with the formula $[H_3Ag^I(H_2O)PW_{11}O_{39}]^{3-}$. Catalytic water oxidation for the evolution of O_2 was carried out on the $[H_3Ag^I(H_2O)PW_{11}O_{39}]^{3-}$. In the presence of $S_2O_8^{2-}$, which can oxidize coordinated metal ions into high oxidation states effectively, the $[H_3Ag^I(H_2O)PW_{11}O_{39}]^{3-}$ oxidized to $[H_3Ag^{II}(H_2O)PW_{11}O_{39}]^{2-}$ and a small number of $[H_3Ag^{III}OPW_{11}O_{39}]^{3-}$ POM anions. These oxidation processes in POM anions form the basis of the mechanism for the evolution of oxygen. The water oxidation catalyst (WOC) tests discussed in this work show that lacunary POMs play important roles in the transmission of both electrons and protons as well as in improvements in redox performances and stabilizing high–oxidation states (2+ and 3+) of silver ions. The photocatalytic activity of $K_3[H_3Ag^IPW_{11}O_{39}]\cdot 12H_2O$ was compared with $[Ag^I(2,2'–$

bpy)NO$_3$] and AgNO$_3$ under the same conditions. The evolution of oxygen was significantly higher when the POM anion was involved, while no O$_2$ production was observed in the case of [Ag^I(2,2′–bpy)NO$_3$] [114]. In another work, this group also investigated the electrocatalytic and photoelectrocatalytic effects of [H$_3$Ag^{I}PW$_{11}$O$_{39}$]$^{3-}$ on water oxidation when it was immobilized on a TiO$_2$ electrode. In order to investigate the effect of this Ag^I–substituted polyion on water oxidation activity, three electrocatalytic systems, namely, AgPW$_{11}$–TiO$_2$/ITO and AgNO$_3$–TiO$_2$/ITO electrodes, as well as a single TiO$_2$/ITO electrode, were evaluated under identical conditions. The current density of the AgPW$_{11}$–TiO$_2$/ITO electrode was higher than the current densities for the other two electrodes [115]. [H$_3$Ag^I(H$_2$O)PW$_{11}$O$_{39}$]$^{3-}$ was then used in reversible redox reactions for LiS featuring electrode architectures. Here, the addition of the Ag^I ion as a hetero-metal ion was able to act as a Lewis acid site to further enhance the adsorption of the S-moieties, and the terminal oxoligands in the POM anion interacting with the Li cations in the Li$_2$Sn species were regarded as Lewis acid sites. The results of the experiments and calculations confirmed that the {Ag^{I}PW$_{11}$O$_{39}$] POM anion enhanced the redox reversibility of the S atom and polysulfides throughout the battery [116]. Silver forms large cluster units in combination with POMs. Sandwich–type POM {[Ag$_{42}$(CO$_3$)(C≡CtBu)$_{27}$(CH$_3$CN)$_2$][CoW$_{12}$O$_{40}$]$_2$}$^+$ has 42 silver ions encapsulated within two [CoW$_{12}$O$_{40}$] POM units. The Ag$_{42}$ cluster is coordinated by 27 tertbutylethynyl ligands and two acetonitrile ligands, and the compound has a CO$_3^{2-}$ anion at its center. The silver cluster [Ag$_{14}$(C≡CtBu)$_{12}$][BF$_4$]$_2$, in combination with α–(nBu$_4$N)$_5$[HCoW$_{12}$O$_{40}$] at a 3:2 molar ratio (or {[Ag$_3$(C≡CtBu)$_2$][BF$_4$]·0.6H$_2$O}$_n$ and α–(nBu$_4$N)$_5$[HCoW$_{12}$O$_{40}$] at a 7:1 molar ratio) has been used for the preparation of the gigantic {[Ag$_{42}$(CO$_3$)(C≡CtBu)$_{27}$(CH$_3$CN)$_2$][CoW$_{12}$O$_{40}$]$_2$}$^+$ compound in a one-pot reaction (Fig. 16) [117].
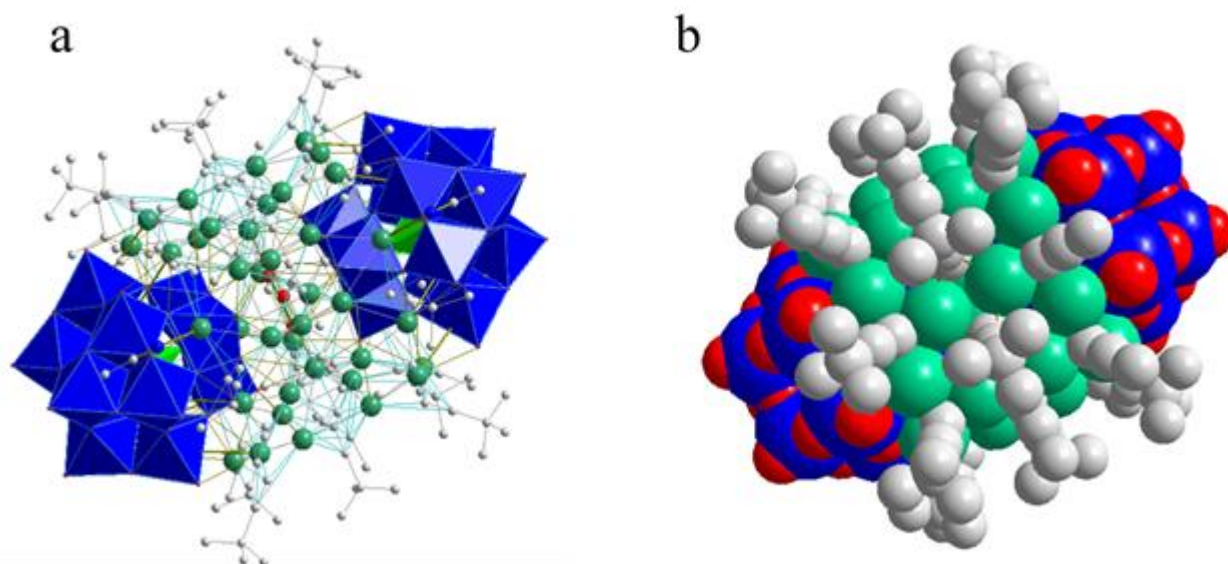
Fig. 16. The $\{[Ag_{42}(CO_3)(C\equiv CtBu)_{27}(CH_3CN)_2][CoW_{12}O_{40}]_2\}^+$ structure presented in (a) polyhedra form, and (b) space-filling form. Color code: $\{WO_6\}$ = blue; $\{CoO_4\}$ = green; Ag = sea green; O = red; C = gray.

Encapsulating a silver cluster $\{Ag_4\}$ between two lacunary POM fragments led to the formation of a sandwich–type cluster. As mentioned previously, metals containing POM anions have been synthesized by *via* the reactions of alkali metal salts of lacunary POMs and the corresponding metal salts in aqueous media. However, in such media, acidic conditions may result in the decomposition of the lacunary POMs. Therefore, in 2012, in order to overcome this problem, the Kikukawa and Mizuno group initiated one of these reactions in an organic medium. The reaction of two lacunary $[\gamma–SiW_{10}]^{8-}$ Keggin-type POM anions and AgOAc in acetone led to the formation of a TBA$_8$[Ag$_4$(DMSO)$_2$(γ–H$_2$SiW$_{10}$O$_{36}$)$_2$]·2DMSO·2H$_2$O cluster. Encapsulated within two SiW$_{10}$ subunits, the silver cluster contained two Ag atoms coordinated to two DMSO molecules in the middle of the cluster, while the other two Ag atoms were bridged by two SiW$_{10}$ subunits in a slightly distorted square-planer environment. The cluster catalyzed the hydrolytic oxidation of various structurally diverse silanes into their corresponding silanols effectively [118]. Another sandwich-type TBA$_8$[Ag$_6$(γ–H$_2$SiW$_{10}$O$_{36}$)$_2$]·5H$_2$O was obtained in the reaction of

TBA$_4$H$_4$[γ-SiW$_{10}$O$_{36}$] (TBA = tetra–n–butylammonium) with AgOAc while using dimethylphenylsilane as a reductant in acetone. The octahedrally-shaped hexasilver cluster was encapsulated within two [γ–H$_2$SiW$_{10}$O$_{36}$]$^{6-}$ fragments. In the [Ag$_6$]$^{4+}$ cluster in the compound, two Ag atoms were coordinated to the two oxygen atoms of the central {SiO$_4$} tetrahedron, and the other four Ag atoms were bridged by two SiW$_{10}$ subunits (Fig. 17) [119].
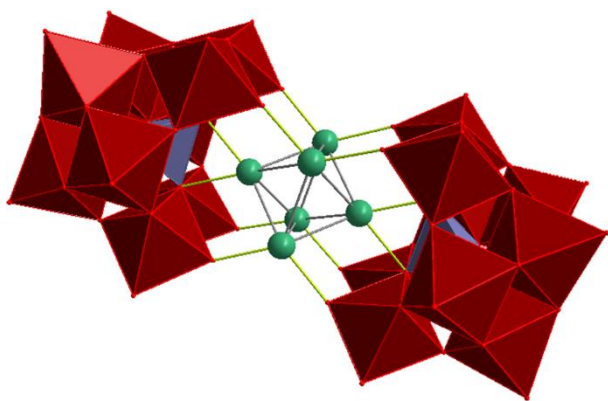
Fig. 17. Structure of [Ag$_6$(γ-H$_2$SiW$_{10}$O$_{36}$)$_2$]$^{8-}$. Color code: {WO$_6$} = dark red; {PO$_4$} = blue gray; Ag = sea green.

Alternatively, in another structure with the formula {[Ag$_7$(H$_2$biim)$_5$][PW$_{11}$O$_{39}$]}·Cl·H$_3$O, (H$_2$biim = 2,2′–biimidazole), two silver clusters, both {Ag$_6$}, were encapsulated by two neighboring monolacunary Keggin-type anions, PW$_{11}$ (two of the six silver atoms had a 50% occupancy rate), and an {Ag$_4$} cluster with four crystallographically–unique Ag^I ions was connected to four H$_2$biim molecules *via* Ag−N bonds. Here, the {Ag$_4$} cluster in the compound acted as a counteraction [120]. One of the largest isolated silver(I) alkynyl cluster reported was Jiang and colleagues' silver alkynyl cluster [Ag$_{70}$(PW$_9$O$_{34}$)$_2$(^{t}BuC≡C)$_{44}$(H$_2$O)$_2$][BF$_4$]$_8$·2[BMIm]BF$_4$·3H$_2$O (BMIm = 1-butyl-3-methylimidazolium), which was prepared in a reaction of AgC≡CBu^t, AgCF$_3$SO$_3$ with

$[A\text{-}\alpha\text{-}PW_9O_{34}]^{9-}$ in $[BMIm]BF_4$ under ionothermal conditions. The compound consisted of two trilacunary $[A–\alpha–PW_9O_{34}]^{9-}$ fragments, and a cationic cluster comprised an Ag_{70} shell encapsulating two $[PW_9O_{34}]^{9-}$ cores. Ten silver atoms were located in the middle of the cluster and were sandwiched by two $[PW_9O_{34}]^{9-}$ subunits. These silver atoms were coordinated to the vacant sites in the POM anions. The two middle Ag atoms were bridged by two H_2O molecules in a slightly distorted square-planar environment, and 44 alkynyl ligands enclosed the silver cluster and POM complex (Fig. 18) [121].
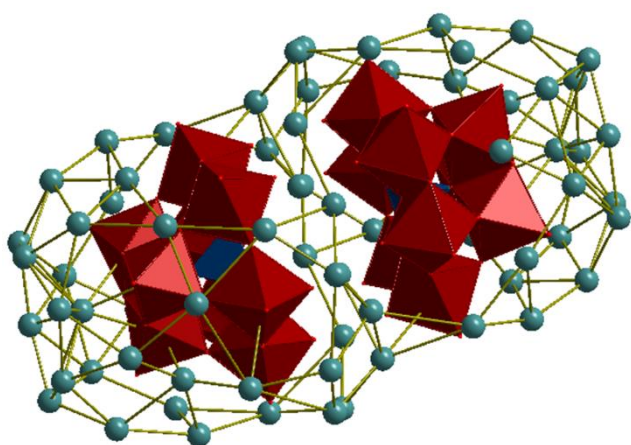

Fig. 18. Structure of $[Ag_{70}(PW_9O_{34})_2(^tBuC\equiv C)_{44}(H_2O)_2][BF_4]_8\cdot2[BMIm]BF_4\cdot3H_2O$. Color code: $\{WO_6\}$ = dark red; $\{PO_4\}$ = dark blue; Ag = sea green.

Another Ag_{42} cluster encapsulating POMs $[Ag_{42}\{Eu(W_5O_{18})_2\}(^tBuC\equiv C)_{28}C_{l4}][OH]\cdot H_2O$ was synthesized *via* the reaction of the starting materials $Na_9[Eu(W_5O_{18})_2]\cdot xH_2O$, $[^tBuC\equiv CAg]_n$ and $AgCF_3SO_3$. The 42 silver atoms formed a cage that completely surrounded the anionic part. In other words, the dimeric $Eu(W_5O_{18})_2$ anion acted as a template to induce the formation of the surrounding Ag_{42} cage *via* Ag–O bonds, and the whole silver cage was stabilized by alkynyl ligands and four Cl atoms situated above and below the silver cage. Fluorescence–active EuW_{10} entrapped in a silver(I)–alkynyl shell showed similar emission peaks for the free EuW_{10} anion but with slight changes in relative intensity. Because it reduced the energy loss due to the interactions between EuW_{10} and

the solvents effectively during the silver alkynyl shell's emission process, the POM anion's fluorescent intensity was higher than that of EuW_{10} during all transitions [122]. The largest known silver(I) alkynyl cluster encapsulating POMs, $[Ag_{72}(EuW_{10}O_{36})_2(^tBuC\equiv C)_{48}C_{12}\cdot 4BF_4]$, was isolated under solvothermal conditions [123]. The silver cluster in the tungsten cluster compound was prepared *via* the self-organization of two $\{Te_3W_{38}\}$ units around a single chloride template encapsulated within the central $\{Ag_{12}\}$ core of the cluster, producing a $\{Ag_{12}\}$–in–$\{W_{76}\}$ cluster–in–cluster. $Na_2WO_4\cdot 2H_2O$, Na_2TeO_3, 2–dimethylaminoethanol $AgNO_3$, and $NaCl$ were the starting materials in solution that were used for preparing the compound [124]. In 2016, two fully inorganic silver–containing POMs in a new POM class, namely, the polyoxopalladate class, were introduced by the Kortz group [125]. The descriptions of these compounds are provided in Section 4.

3.5. Osmium

The nitrido ligand stabilizes the high–valent transition-metals better than the oxo ligand due to the addition of the anion charge effect and local effects in the TM–N and TM–O orbitals. Therefore, there have been a few reports related to the Os-containing POM anions with Os-nitrogen bonds [126].

The reaction of $[PW_{11}O_{39}Ru^{II}NO]^{4-}$ with hydroxylamine on the path toward $[PW_{11}O_{39}Ru^{III}H_2O]^{4-}$ has a ruthenium−dinitrogen intermediate $[PW_{11}O_{39}Ru^{II}(N_2)]^{5-}$ that has been detected by ^{31}P NMR and ESI-MS. The Ru-dinitrogen POM complex is unstable and oxidizes, yielding the aquated $[PW_{11}O_{39}Ru^{III}H_2O]^{4-}$ structure. During this process, it is difficult to separate the intermediate from the mixtures of isostructural byproducts experimentally. Therefore, to better detect the nature of the intermediate in this process, a DFT method utilizing the M06L functional was used on the $[PW_{11}O_{39}M^{II}(N_2)]^{5-}$ (M = Ru, Os, Re, Ir) analogue intermediates. IR spectroscopy is useful in detecting structural differences within this context. The DFT–derived IR spectra of the ruthenium−dinitrogen POM complex was used to examine the shifts and the presence or absence of certain

bands. A comparison of calculated and experimental vibrational frequencies was carried out. There was a significant shift in the IR band corresponding to P−Oa motion upon the replacement of NO^+ with N_2, and the presence of the strong IR band at 1850 cm^{-1} corresponded to the stretch vibration of the NO^+ moiety (1850 cm^{-1} (experimental) vs 1884 cm^{-1} (calculated)). Furthermore, the absorption peak corresponding to the stretch vibrations of the N−N bond calculated using the DFT-derived IR spectra, along with some other methods, confirmed the presence of the intermediate $[PW_{11}O_{39}Ru^{II}(N_2)]^{5-}$. The exploration of metal−dinitrogen bonding with the DFT calculation method indicated that although all these POM complexes have similar metal−dinitrogen moieties, their M−N and N−N distances differ considerably. The optimized metal−nitrogen bond distances decrease in the following order: Ir > Ru > Re > Os. The metal−dinitrogen interactions and optimized N−N bond distances increase in the following order: Ru < Ir < Os < Re. Hence, the Os−dinitrogen POM complex has the strongest Os–N interaction and is the most active in terms of N_2 adsorption, as it has considerable adsorption energy [46].

Typically, TM amine complexes can be added to POMs easily using metal salts and amines as starting materials under hydrothermal conditions. However, doing so under conventional solution conditions is relatively difficult. Therefore, M−amine complexes can be used to facilitate a substitution process for the POMs when using conventional solution syntheses. The Proust and Kwen groups used this method in the reaction of monovacant species with Os-nitrido monomers and formed a nitrido derivative of Keggin−type anion (n-Bu₄N)₄[PW₁₁O₃₉(Os^{VI}N)]. A ^{14}N NMR signal was observed for the nitrido ligand in the hybrid. This derivative was the first example of osmium−nitrido being inserted into a POM [127]. The influence of the osmium−nitrido site on the electronic and redox properties of the $[PW_{11}O_{39}(OsN)]^{2-}$ POM anion was investigated by means of DFT calculations and compared with the results for $[PW_{12}O_{40}]^{3-}$. The LUMOs in fully oxidized $[PW_{11}O_{39}(OsN)]^{2-}$ are mainly concentrated on the Os centers, and the contribution from the tungsten atoms is quite small. The LUMO energy in

$[PW_{11}O_{39}(OsN)]^{2-}$ is lower than that in $[PW_{12}O_{40}]^{3-}$, and the HOMO-LUMO gap in the Os-containing POM anion is smaller than that of $[PW_{12}O_{40}]^{3-}$. Therefore, the electron transition between HOMO and LUMO of the nitrido-functionalized POM species $[PW_{11}O_{39}(OsN)]^{2-}$ is much easier compared with that transition in Keggin-type $[PW_{12}O_{40}]^{3-}$ [128]. The binding ability of monolacunary $[\alpha-PW_{11}O_{39}]^{7-}$ toward the $\{Os(DMSO)_3(H_2O)\}^{2+}$ and $\{Os(\eta^6-p-arene)(H2O)\}^{2+}$ fragments was investigated by Proust, Ge´rard and colleagues, who synthesized $([PW_{11}O_{39}\{Os(DMSO)_3(H_2O)\}]^{5-}$ and $[PW_{11}O_{39}\{Os(\eta^6-p-cym)(H_2O)\}]^{5-}$ and characterized these products with NMR spectroscopy [129]. The reaction of monolacunary Wells−Dawson type polyoxotungstate in α_1 and α_2 forms and monolacunary $\alpha-$Keggin−type polyoxotungstates with the nitrido complex $[OsCl_4N]^-$ in a water/methanol mixture and subsequent precipitation with $(Bu_4N)Br$ produced $[\alpha_1-P_2W_{17}O_{61}\{Os^{VI}N\}]^{7-}$, $[\alpha_2-P_2W_{17}O_{61}\{Os^{VI}N\}]^{7-}$ Wells−Dawson type structures, and $[\alpha-PW_{11}O_{39}\{Os^{VI}N\}]^{4-}$ Keggin−type derivatives as tetrabutylammonium salts. ^{183}W and ^{15}N NMR, EPR, IR, and UV–Vis spectroscopies, electrochemistry and ESI mass spectrometry were used to characterize the clusters [130].

3.6 Iridium

$[XW_{11}O_{39}Ir^{IV}(H_2O)]^{n-}$ (X = B, Si, Ge, P), $[PMo_{11}O_{39}Ir^{IV}(H_2O)]^{3-}$, and α_2- $[P_2W_{17}O_{61}Ir^{IV}(H_2O)]^{6-}$ were produced in solution *via* the reaction of H_2IrCl_6 with the appropriate lacunary POMs by Liu and colleagues as examples of Ir substitutions into lacunary POM anions accomplished *via* mono−iridium substitution, in which an Ir atom is attached to the oxygen atom of water. The above formulas were confirmed by ^{31}P and ^{183}W NMR spectroscopy. The M−substituted Wells−Dawson type POMs (M = Ir, Pd and Pt) have been investigated as oxygen transfer agents for H_2O_2 to a series of primary allylic alcohols for the generation of epoxides [25, 99]. Sun and colleagues have shown that the latter compounds are excellent catalysts for the electroreduction of the nitrite ion to nitrosyl since all of these Ir−substituted POMs have high electrocatalytic activity, even

though the heteroatoms in the heteropolyanions differ and the unsubstituted parent anions show no catalytic activity [131].

In 2009, Cao and colleagues reported the first structurally−characterized iridium−substituted POM, $K_{14}[(IrCl_4)KP_2W_{20}O_{72}]\cdot23H_2O$ (Fig. 19a). When they used $IrCl_3$ and $Na_9[A−\alpha−PW_9O_{34}]$ as starting materials, the reaction formed colorless tungsten complexes with no Ir atoms incorporated into the polytungstates. This result was due to the hydrolytic degradation of $[PW_9O_{34}]^{9−}$ before its reaction with inert Ir^{3+} ions. Therefore, they decided to try alternative methods. The $IrCl_3$ was added to the $[APW_9O_{34}]^{9−}$ anion, which was generated from the reaction of $K_{10}[\alpha_2−P_2W_{17}O_{61}]$ and K_2WO_4 in situ, instead of using its isolated sodium salt. The latter compound was tested as a catalyst in the generation of O_2 *via* the oxidation of water by strong oxidants, such as $[Ru(bpy)_3]^{3+}$, which was reduced to $[Ru(bpy)_3]^{2+}$ [132]. To overcome these obstacles, a continuous-flow apparatus was used to produce a new Ir(III)−containing POM cluster. Needle−like black crystals of $K_{12}Na_2H_2[Ir_2Cl_8P_2W_{20}O_{72}]\cdot37H_2O$ (Fig. 19b) were obtained *via* a reaction of $Na_8[HPW_9O_{34}]$ and $IrCl_3$ and crystallized in the orthorhombic space group *Pnnm*. The crystal structure comprised POM anion $[Ir_2Cl_8P_2W_{20}O_{72}]^{16−}$, K^+, Na^+, H^+ cations, and lattice waters. Two trivacant Keggin−type $[PW_9O_{34}]^{9−}$ building blocks, two $[IrCl_4]$ fragments, and two $[W^{VI}O_2]$ fragments formed an S−shaped structure. The application of a flow-type reactor enabled the synthesis of crystalline materials, which would have been difficult to achieve using traditional methods. The catalytic activities of $K_{12}Na_2H_2[Ir_2Cl_8P_2W_{20}O_{72}]\cdot37H_2O$ were investigated when catalyzing the electro-oxidation of ruthenium tris−2,2′−bipyridine $[Ru(bpy)_3]^{2+/3+}$. It could potentially be used to drive the oxidation of water under visible–light irradiation with the Ru-complex *via* the acceleration of the oxidation of $[Ru(bpy)_3]^{2+/3+}$ [133]. When their attempts to synthesize $[PW_{11}O_{39}Ir(H_2O)]^{4−}$ *via* the reaction of the precursors $[PW_{11}O_{39}]^{7−}$ and $IrCl_3/K_2[IrCl_6]$ failed to produce high yields, Sokolov and colleagues used $K_2[IrF_6]$ as the Ir source and $K_7[PW_{11}O_{39}]\cdot7H_2O$ (yield 90%) as well as $K_2[IrF_6]$and trilacunary $Na_9[\alpha−PW_9O_{34}]\cdot7H_2O$,

(yield 81%). The structure was characterized by *via* multinuclear ^{31}P and ^{183}W NMR spectroscopy and ESI−mass spectrometry as well as cyclic voltammetry, while the detection of the minor formation of the methyl derivative was carried out *via* an ESI-MS-based methodology [134].
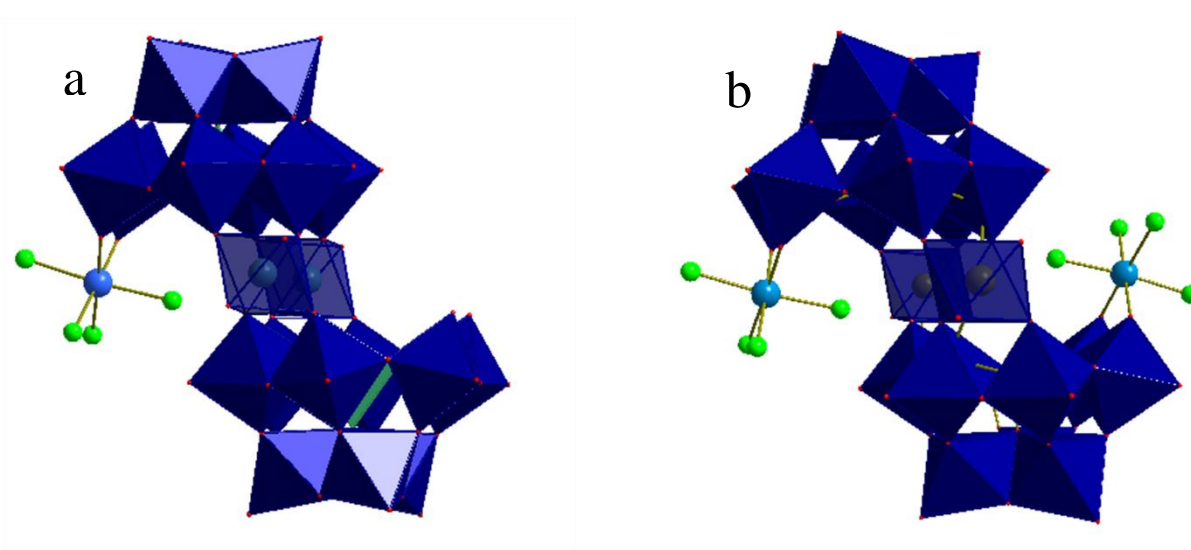

Fig. 19. Structures of (a) $[(IrCl_4)KP_2W_{20}O_{72}]^{14-}$, and (b) $[Ir_2Cl_8P_2W_{20}O_{72}]^{16-}$. Color code: $\{WO_6\}$ = dark blue; Ir = blue; Cl = green.

In reactions of $[PW_{11}O_{39}Ir(H_2O)]^{4-}$ with $(CH_3)_3SnCl$ and other metal−organic species, it was shown that only the Ir−CH_3−containing POM anion with the formula $[PW_{11}O_{39}IrCH_3]^{5-}$ was formed under identical conditions [135]. As mentioned previously, the reaction of $IrCl_6$ with $[PW_{11}O_{39}]^{7-}$ led to a low yield of the $[PW_{11}O_{39}Ir^{IV}(H_2O)]^{n-}$ POM anion, while the same reaction with the IrF_6 precursor resulted in a high yield of the same compound. Therefore, attempts were made to find an alternative high−yield and operationally−simpler synthetic routes towards Ir−Cl−substituted POMs. Sokolov and colleagues carried out several experiments that

used $K_3[IrCl_6]$ as the iridium source. Their experiments showed that Li^+ salts were required to provide a high yield of $[PW_{11}O_{39}IrCl]^{5-}$ because it prevented the collapse of the lacunary form into a closed $[PW_{12}O_{40}]^3$ structure. The reaction process involving the $[PW_{11}O_{39}RhCl]^{5-}$ POM anion, NaN_3, $NaNO_2$, and NaSCN was investigated *via* an ESI-MS analysis. It showed that $NaNO_2$ and NaN_3 did not succeed in making replacements and that the $[PW_{11}O_{39}IrCl]^{5-}$ precursor was the only POM anion species in the resulting solution. Just $[PW_{11}O_{39}Ir(SCN)]^{5-}$ was obtained under similar hydrothermal conditions, and these results revealed that in this series of reactions, the Ir-substituted cluster showed a lower reactivity towards ligand−substitution reactions compared to its rhodium homologue[92].

Metal-substituted Wells−Dawson type $[K/(n-C_4H_9)_4N]_{10-n}[P_2W_{17}O_{61}M(H_2O)]$ ($M^{n+} = Ir^{4+}$, Ru^{3+}, and Pd^{2+}) anions have been investigated as chemoselective and regioselective oxygen transfer agents for H_2O_2 to the allylic alcohols to generate the corresponding epoxides under biphasic reaction conditions. It should be noted that in this study, some first-row transition metal elements were also evaluated. These M−substituted species had different levels of activity. In other words, the type of substituted metal affects the activity levels of catalysts [99].

3.7. Platinum

$[PW_{11}O_{39}Pt]^{5-}$, one of the most important Pt−containing POM anions, which is used in many cases as a starting material in the preparation of various compounds, was first obtained in a reaction of $[PtCl_4]^{2-}$ with $[PW_{11}O_{39}]^{7-}$ in aqueous solution and investigated *via* electronic, IR, ^{31}PNMR, and ^{195}PtNMR spectroscopies. The UV−Vis spectra of the solutions containing Pt^{II} and PW_{11} indicated that $[PW_{11}O_{39}Pt]^{5-}$ was the predominant product in solution. $[PW_{11}O_{39}Pt]^{5-}$ was investigated as an oxidation catalyst in the oxidation of benzene with an O_2/H_2 gaseous mixture [97]. Tourn and colleagues reported that $[WM_3(H_2O)_2(MW_9O_{34})_2]^{12}$ ($M = Zn^{II}$, Co^{II}) can be transformed into a substitution derivative by replacing the M atoms (two or three for Zn, two only for Co) by metal

cations, including Pd^{II} and Pt^{II}, and some of the first-row transition metals [136]. The sandwich-type structure $\{[WZnPd^{II}_2(H_2O)_2][(ZnW_9O_{34})_2]\}^{2-}$ and $\{[WZnPt^{II}_2(H_2O)_2][(ZnW_9O_{34})_2]\}^{12-}$ POM anions were again prepared by Neumann and colleagues in 1995, who exchanged labile zinc atoms from the isostructural $Na_{12}\{[WZn_3(H_2O)_2](ZnW_9O_{34})_2]\}$ for platinum atoms as the starting material. The sandwich−type structure was characterized by IR, UV−Vis spectroscopy, and single−crystal X−ray analysis and investigated as a catalyst in the oxidation of alkanes and alkenes with peroxides. They also used this cluster selectively to catalyze the reaction in which chiral allylic alcohols transfer to epoxy alcohols with 30% hydrogen peroxide under mild conditions in an aqueous/organic biphasic system [137].

The reaction of $K_2Pt(OH)_6$ and monolacunary $K_8[\alpha-SiW_{11}O_{39}]\cdot13H_2O$ in the presence of $CH_5N_3\cdot HCl$ led to the formation of the α−Keggin−type doubly−Pt^{IV}−substituted silicotungstate $(CH_6N_3)_8[\alpha-SiPt_2W_{10}O_{40}]\cdot6H_2O$. A single−crystal X−ray analysis indicated that the compound contained a novel α-Keggin-type heteropolyanion in which two of the addenda atoms were replaced by Pt atoms. W and Pt atoms occupy the same coordinates with occupancy fractions of 5/6 (W) and 1/6 (Pt) [138]. The Knoth-type tungstophosphate dimer $K_7Na_9[Pt(O)(H_2O)(PW_9O_{34})_2]\cdot21.5H_2O$ was prepared and isolated at room temperature as air-stable brown crystals by the Hill group in 2004. A single−crystal X−ray analysis of the crystals at 193 K and neutron diffraction at 30 K confirmed the existence of short platinum-oxo linkages and that the bond excluded the hydrogen atoms of the terminal oxygen [139]. In 2008, Kortz and colleagues prepared and structurally characterized a mono−platinum(IV) derivative of the decavanadate ion $[H_2Pt^{IV}V_9O_{28}]$. This derivative was the first transition−metal-substituted decavanadate derivative and the first platinum(IV) −containing polyoxovanadate that was prepared by the reaction of $Na_2[Pt(OH)_6]$ with $NaVO_3$ in aqueous solution. Here, Pt^{IV} replaced one of the two central vanadiums, ^{51}V NMR, and, for first time, ^{195}Pt NMR spectroscopy was used successfully to characterize it in solution. The ^{195}Pt NMR measurement displayed

the expected singlet for the POM anion at d = 3832 ppm. The corresponding [195]Pt NMR signal for the precursor $Na_2[Pt(OH)_6]$ appeared significantly more up−field (3294 ppm) [140]. Four individual peaks in the experimental [51]V NMR spectrum corresponded to the four nonequivalent vanadium atoms [141].

Kato and colleagues reported a reaction of Keggin-type monolacunary polyoxotungstate, $[\alpha\text{-}PW_{11}O_{39}]^{7-}$ with $cis−Pt(NH_3)_2Cl_2$ in an aqueous solution, which yielded a di−pt[II] containing the $[(CH_3)_4N]_3[\alpha\text{-}PW_{11}O_{39}\{cis−Pt(NH_3)_2\}_2]$ POM anion. During the formation of $[\alpha\text{-}PW_{11}O_{39}\{cis\text{-}Pt^{II}(NH_3)_2\}_2]^{3-}$, an intermediate species was observed with the suggested formula of the mono−pt[II]−coordinated POM anion $[\alpha\text{-}PW_{11}O_{39}\{cis−Pt(NH_3)_2\}]^{5-}$. It is possible to obtain this product with a relatively high abundance ratio *via* another method, as well [142, 143]. The titular compound in cesium salt, $Cs_3[\alpha−PW_{11}O_{39}\{cis−Pt(NH_3)_2\}_2]\cdot8H_2O$, was obtained *via* the addition of CsCl to the mixture of *cis*−platinum and the monolacunary Keggin−type POM, and its structure was determined *via* single−crystal X−ray analysis. The findings concerning the positions of the platinums stated previously were confirmed (Fig. 20)[144]. The photocatalytic performances of $[(CH_3)_4N]_3[\alpha−PW_{11}O_{39}\{cis−Pt(NH_3)_2\}_2]$, $Cs_3[\alpha\text{-}PW_{11}O_{39}\{cis−Pt(NH_3)_2\}_2]\cdot8H_2O$, $[cis−Pt(NH_3)_2]^{2+}$, $[\alpha−PW_{11}O_{39}]^{7-}$, and a mixture of *cis*−platinum and $Na_3[\alpha−PW_{12}O_{40}]\cdot15H_2O$ were investigated for the identification of possible sensitizers and co−catalysts for the evolution of hydrogen from an EDTA·2Na (ethylenediamine tetraacetic acid disodium salt) aqueous solution under visible–light irradiation in the presence of TiO_2. In the case of $Cs_3[\alpha−PW_{11}O_{39}\{cis−Pt(NH_3)_2\}_2]\cdot8H_2O$, after 6 h, the amount of H_2 evolved increased to 171 µmol, and the turnover number (TON) reached 426. The catalytic activities of $[(CH_3)_4N]_3[\alpha\text{-}PW_{11}O_{39}\{cis−Pt(NH_3)_2\}_2]$ were similar to those of $Cs_3[\alpha−PW_{11}O_{39}\{cis−Pt(NH_3)_2\}_2]$. As for the *cis*-platinum species under the same conditions, its TON was similar to those for the POM anions and reached 445. However, ^{31}P NMR spectroscopy revealed that the stability of the platinum sites was improved remarkably by the coordination with an $\alpha−$Keggin-type monolacunary

polyoxotungstate. No hydrogen evolution was observed when $K_7[\alpha-PW_{11}O_{39}]\cdot 13H_2O$ was used as a photocatalyst. Due to the difficulty in reducing protons for TiO_2, the platinum sites act as sensitizers and co−catalysts[144].
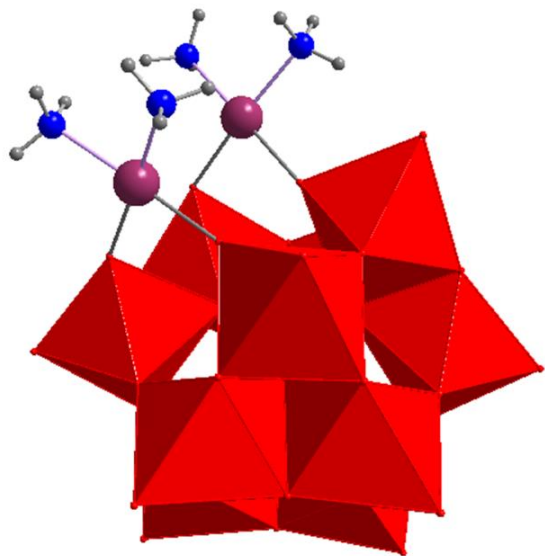
Fig. 20. Structure of $[\alpha-PW_{11}O_{39}\{cis\text{-}Pt(NH_3)_2\}_2]^{3-}$. Color code: $\{WO_6\}$ = dark red; Pt = plum; N = blue; H = gray.

By Cao and colleagues, the latter compound, $Cs_3[\alpha-PW_{11}O_{39}\{cis-Pt(NH_3)_2\}_2]$, was modified on the commercial TiO_2 surface, which resulted in the formation of a composite with formula TiO_2-$SiNH_2$-$PW_{11}Pt_2$, and photocatalytic performance of the composite for H_2 evolution was investigated. In this work, the photocatalytic performance of TiO_2-Pt, TiO2, $PW_{11}Pt$ and TiO_2-$SiNH_2$-PW_{11} was evaluated under the same conditions. The result indicated that photocatalytic efficiency of TiO_2-$SiNH_2$-$PW_{11}Pt_2$ nanoparticles is higher than other compounds tasted in this study. In addition, TiO_2-$SiNH_2$-$PW_{11}Pt_2$ shows high stability in photocatalytic hydrogen evolution reaction. The possible electron transport path of TiO_2-$SiNH_2$-$PW_{11}Pt_2$ in photocatalytic hydrogen evolution process is illustrated in schematic 2.
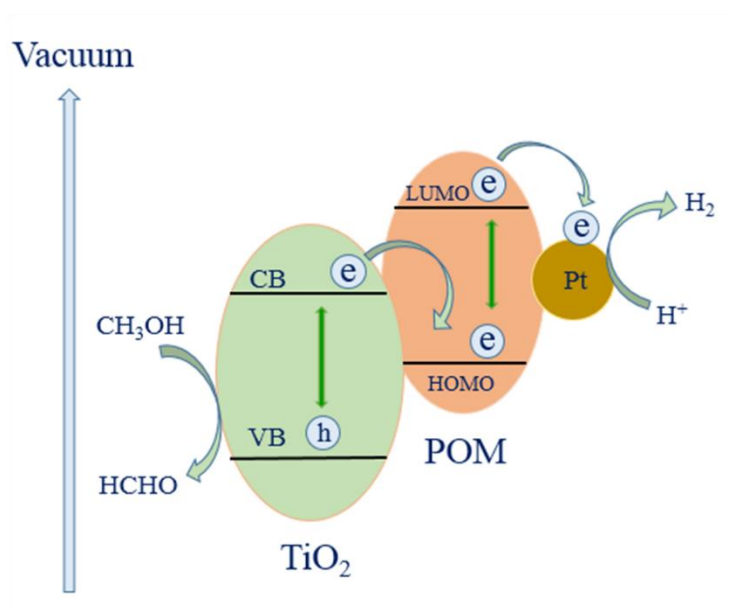
Schematic 2. Possible mechanism of photocatalytic reaction in the presence of TiO_2-$SiNH_2$-$PW_{11}Pt_2$.

Pt^{2+} species fixed in the $PW_{11}Pt_2$ was reduced to Pt^0 by photoreduction and acts as an active site for hydrogen evolution. POMs can trap photoinduced electrons, increasing the electron mobility rate from POMs to Pt^0. Due to its unique valence electron state, Pt^0 has a very strong adsorption capacity for protons in the solution [145]. In another experiment, in a reaction of $[\alpha-PW_{11}O_{39}]^{7-}$ with $[cis-Pt(Me_2ppz)]^{2+}$ (Me_2ppz = N,N′−dimethylpiperazine), researchers prepared $[(CH_3)_4N]_4H[\alpha-PW_{11}O_{39}\{cis-Pt^{II}(Me_2ppz)\}]\cdot 5H_2O$. The POM anion $[\alpha-PW_{11}O_{39}\{cis-Pt^{II}(Me_2ppz)\}]^{5-}$ was more stable in dimethylsulfoxide and water than the $[\alpha-PW_{11}O_{39}\{cis-Pt(NH_3)_2\}]^{5-}$. The synthesized clusters were characterized by elemental analysis, TG/DTA, FT−IR, UV–Vis, and ^1H, ^{31}P, ^{183}W, and ^{159}Pt NMR spectroscopies. In the structures of the synthesized POM anions, $[(CH_3)_4N]_3[\alpha-PW_{11}O_{39}\{cis-Pt(NH_3)_2\}_2]$, the two *cis*-platinum(II) moieties $[cis-Pt(NH_3)_2]^{2+}$ were grafted onto the monolacunary POM by two oxygen atoms occupying monovacant sites in $[\alpha-PW_{11}O_{39}]^{7-}$ [146]. Crystallographically-characterized Pt−N−containing POM anions were reported by the same group, who created them with monolacunary Wells−Dawson type POMs with different heteroatoms

(Al/B/Ge), different N donor fragments, and clusters with different counterions, namely, $[(CH_3)_4N]_4H[\alpha-AlW_{11}O_{39}\{cis-Pt(NH_3)_2\}_2]\cdot11H_2O$,

$[(CH_3)_4N]_4H[\alpha-BW_{11}O_{39}\{cis-Pt(NH_3)_2\}_2]\cdot9H_2O$, $Cs_4[\alpha-GeW_{11}O_{39}\{Pt(bpy)\}_2]\cdot10H_2O$, $Cs_{3.5}H_{0.5}[\alpha-GeW_{11}O_{39}\{Pt(phen)\}_2]\cdot3H_2O$ (phen = 1,10−phenanthroline), and $Cs_6[\alpha_2-P_2W_{17}O_{61}\{cis-Pt(NH_3)_2\}_2]\cdot13H_2O$. The latter compounds were used as photocatalysts for the evolution of H_2 from aqueous triethanolamine (TEOA) solution under light irradiation. The results indicated that $Cs-GeW_{11}-Pt$-bpy and $Cs-GeW_{11}-Pt$-phen exhibited the lowest activities and that the Wells−Dawson−type POMs exhibited the highest activity among the tested compounds. The experiments showed that the counter−ions did not affect the photocatalytic activities of the samples. However, the type of ligand affected the photocatalytic performances of the compounds, with the phenanthroline and bipyridine ligands producing the lowest yields. However, the effect of the POM skeletal structure was more pronounced. In general, for this series of compounds, the characterization results indicated that a platinum(II) −L moiety was coordinated to two oxygen atoms in a monovacant site of the lacunary POM [143]. Hydrogen production from water under visible–light irradiation was studied in another photocatalytic system constructed using Eosin Y (EY), $Cs_3[\alpha\text{-}PW_{11}O_{39}\{cis-Pt(NH_3)_2\}_2]\cdot8H_2O$, $K_5[\alpha-SiW_{11}\{Al(OH_2)\}O_{39}]\cdot7H_2O$, and TiO_2, in aqueous triethanolamine (TEOA) solution, which served as an electron donor. Although the addition of Al-containing silicotungstate to aqueous TEOA solutions containing Pt-containing silicotungstate and EY produced an initial significant decrease in the reaction rate, after 12 h, the system had a high−yield TON that was higher than the TONs produced in the absence of the aluminum compound. In fact, it represented the highest activity obtained for the system. Steady and selective hydrogen production was successfully maintained during long-term light irradiation using the highly effective platinum sites in $Cs_3[\alpha-PW_{11}O_{39}\{cis-Pt(NH_3)_2\}_2]\cdot8H_2O$ in a wide visible region [147].

In 2012, Sokolov and colleagues prepared a dimeric $[Pt_2(W_5O_{18})_2]^{8-}$ isopolytungstate *via* the reaction of $K_2[PtCl_4]$ with $Na_2WO_4 \cdot 2H_2O$. The POM anion consisted of two monolacunary Lindqvist isopoly fragments connected by two square planar Pt(II) centers.[148] The first characterized platinum polyniobates were reported by the Abramov and Sokolov group. Different molar ratios of the starting materials produced different structures. A dimeric complex $[Nb_6O_{19}\{Pt(OH)_2\}]_2^{12-}$ resulted from the reaction of the hexanuclear Lindqvist−type polyoxoniobate $[Nb_6O_{19}]^{8-}$ with $[Pt(OH)_4(H_2O)_2]$ at 1:1 molar ratio. Here, two Pt^{IV} atoms were both coordinated to polyniobate fragments *via* the three oxygen atoms from a $\{Nb_3O_3\}$ face in one $[Nb_6O_{19}]^{8-}$ fragment and one corner oxygen atom from the opposite $[Nb_6O_{19}]^{8-}$ fragment. Using a 1:2 molar ratio for Pt/Nb_6, a sandwich-type complex $[Pt(Nb_6O_{19})_2]^{12-}$ was the first product obtained in the crystallization process, which was carried out using the slow evaporation method [149]. The stability of $Cs_2K_{10}[(Nb_6O_{19})_2\{Pt(OH)_2\}_2] \cdot 13H_2O$ in alkaline aqueous media was studied. When the basicity of the $[(Nb_6O_{19})_2\{Pt(OH)_2\}_2]^{12-}$ solution was increased to pH 12 with NaOH, short-term heating (10min at 60C) of the solution transformed $[(Nb_6O_{19})_2\{Pt(OH)_2\}_2]^{12-}$ into $[Pt(Nb_6O_{19})_2]^{12-}$. Additional heating of the $[(Nb_6O_{19})_2\{Pt(OH)_2\}_2]^{12-}$ solution transformed the latter POM anions into a mixed K^+/Na^+ salt of hexaniobate $K_5Na_3[Nb_6O_{19}] \cdot 9H_2O$ [150].

The butylammonium salt of the $[(n-C_4H_9)_4N]_4H_2[\alpha-SiPtW_{11}O_{40}]$ and potassium salt of the $K_4H_2[\alpha-SiPtW_{11}O_{40}] \cdot 18H_2O$ POM anion were prepared *via* a reaction of $K_8SiW_{11}O_{39}$ with $K_2Pt(OH)_6$ in acidic conditions. Both salts were synthesized in the same manner. However, the salt extracted depended on the salt used in the extraction process, *i.e.*, $(n−C_4H_9)_4NBr$ produced the butylammonium salt, whereas KCL produced the potassium salt of the POM anion [151]. In 2016, Kortz and colleagues reported the first examples of dimeric di−Pt^{II}−containing heteropolytungstates in two isomeric forms, namely, $[anti−Pt^{II}_2(\alpha−PW_{11}O_{39})_2]^{10-}$ and $[syn−Pt^{II}_2(\alpha−PW_{11}O_{39})_2]^{10-}$ (Fig. 21a,b). Both isomers were prepared *via* the reaction of K_2PtCl_4 with $[\alpha−PW_{11}O_{39}]^{7-}$ *anti*−isomer red block

crystals for a yield of 15% (based on W), which was obtained after two weeks. Furthermore, *syn*-isomer, red, needle-like crystals were obtained after the removal of the red block crystals of the *anti*-isomer. The presence of just one ^{31}P−NMR singlet at the initial stage of the reaction and the identification of two sets of singlets after 18h of reaction, along with ESI−MS studies done to detect the reaction stages, indicated that both POM anion isomers formed in the same solution. The two isomeric structures consisted of two square−planar coordinated Pt^{II} centers stabilized by two monolacunary $[\alpha-PW_{11}O_{39}]^{7-}$ Keggin fragments. The main difference between the two configurational isomers was the relative orientation of the two monolacunary $[\alpha-PW_{11}O_{39}]^{7-}$ fragments, which either pointed in opposite directions (*anti*−isomer) or in the same direction (*syn*−isomer) [152].
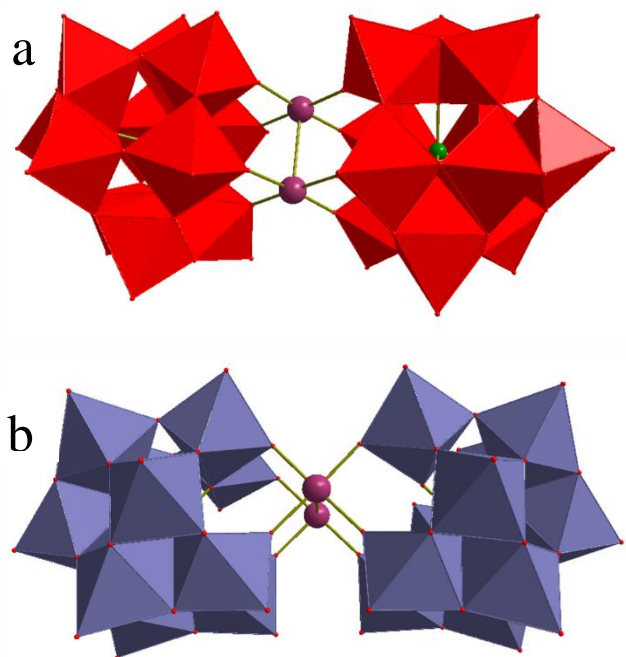

Fig. 21. Structures of the (a) *anti*-isomer and (b) *syn*-isomer of $Pt^{II}_2(\alpha-PW_{11}O_{39})_2]^{10-}$. Color code: {WO$_6$} = red/blue gray; Pt = plum; P = green.

One of the useful techniques for characterizing the chemical compounds in, as well as identifying different structures of, the noble-metal-containing POM anions is NMR spectroscopy. High−resolution solid-state ^{195}Pt MAS−NMR spectroscopy is very useful when working with Pt^{IV}−containing polyoxovanadate clusters. Hence, the Kortz group conducted studies on the feasibility of applying high-resolution solid-state ^{195}Pt MAS−NMR spectroscopy to several Pt^{IV}−containing polyoxotungstates and applying ^{195}Pt and ^{51}V MAS−NMR spectroscopy to a Pt^{IV}−containing polyoxovanadate [153].

Conclusion

In this work, we have discussed the various modes through which a noble metal can contribute to POM chemistry in tradititional forms. In which, the noble metals that participate as heteroatoms in the structures of POMs are listed. The number of compounds included in this category is not high; however, some noble metals, including Ir, Rh, Pt, and Pd, have been used as heteroatoms in the structures of heteropoly anions. Most of the types of POMs synthesized with noble metals as heteroatoms are related to the Anderson−Evans type POM anion. In another section, which has perhaps the most diverse offerings containing most of the noble metals, the noble metals are additives that contribute to the structures of lacunary POMs, leading to the generation of a variety of classical metal-substituted or dimeric, trimeric, or tetrameric metal−substituted POT clusters. It should be noted that ruthenium metal is present in the greatest abundance in synthesized compounds of this kind. Furthermore, the majority of reports on the catalytic and photocatalytic activity of the compounds in this section contain Ru atoms. Ru−containing POMs with unique reversible redox reactions at their Ru sites, as in $[Ru^{IV}_4(\mu-O)_4(\mu-OH)_2(H_2O)_4(\gamma-SiW_{10}O_{36})_2]^{10-}$, can facilitate the catalysis of oxidation reactions, which could possibly benefit from the intrinsically fast electron transfers made possible by, and redox-activated sites in, Ru centers fixed within the cluster set. Section 3 also shows that platinum and palladium atoms show up frequently in the resulting compounds, which exhibit good catalytic and photocatalytic performances. In

Pt−containing POMs, as in $[\alpha−PW_{11}O_{39}\{cis−Pt(NH_3)_2\}_2]$, with excellent photocatalytic efficiency, the stability of the platinum sites was improved remarkably by the coordination with α−Keggin−type monolacunary polyoxotungstate. Due to the difficulty in reducing protons for TiO_2, the platinum sites act as sensitizers and co-catalysts. Alternatively, in the examples of Pd-containing POM anions given, their catalytic activities in numerous hydration, oxidation, epoxidation, and other reactions are discussed.

ACKNOWLEDGMENTS

Abbreviations

POM	polyoxometalate
POT	polyoxotungstate
LPOT	Lacunary polyoxotungstate
PCV	polyoxometalate coacervate vesicle
DPP	dodecaphenylporphyrin
DMSO	dimethyl sulfoxide
TOF	turnover frequency
bpy	2,2'-bipyridine
dpp	2,3-bis(2'-pyridyl)pyrazine
phen	1,10−phenanthroline
DFT	density functional theory
TD-DFT	time-dependent density functional theory
NBO	natural bond orbital
CV	cyclic voltammetry
WOC	water oxidation catalyst
PS	photosensitizer
PSSC	POM sensitized solar cell
Fc	ferrocenyl
CTAB	cetrimonium bromide
SAC	single-atom catalysts
LUMO	lowest unoccupied molecular orbital
TON	turnover number
MO	methyl orange
MB	methylene blue

References

[1] S.S. Wang, G.Y. Yang, Chem. rev. 115 (2015) 4893-4962.

[2] Y. Zhu, Y. Huang, Q. Li, D. Zang, J. Gu, Y. Tang, Y. Wei, Inorg. Chem. 59 (2020) 2575-2583.

[3] X.-F. Su, L.-K. Yan, Z.-M. Su, Inorg. Chem. 58 (2019) 15751-15757.

[4] Y. Zhang, W.-D. Yu, B. Li, Z.-F. Chen, J. Yan, Inorg. Chem. 58 (2019) 14876-14884.

[5] A. Dolbecq, E. Dumas, C.R. Mayer, P. Mialane, Chem. rev. 110 (2010) 6009-6048.

[6] L. Cronin, A. Müller, Chem. Soc. Rev. 41 (2012) 7333-7334.

[7] Y.-Q. Wei, C. Sun, Q.-S. Chen, M.-S. Wang, G.-C. Guo, Chem. Commun. 54 (2018) 14077-14080.

[8] S. Taleghani, M. Mirzaei, H. Eshtiagh-Hosseini, A. Frontera, Coord. Chem. Rev. 309 (2016) 84-106.

[9] M. Arefian, M. Mirzaei, H. Eshtiagh-Hosseini, A. Frontera, Dalton Trans. 46 (2017) 6812-6829.

[10] M. Mirzaei, H. Eshtiagh-Hosseini, M. Alipour, A. Frontera, Coord. Chem. Rev. 275 (2014) 1-18.

[11] M. Alipour, O. Akintola, A. Buchholz, M. Mirzaei, H. Eshtiagh-Hosseini, H. Görls, W. Plass, Eur. J. Inorg. Chem. 2016 (2016) 5356-5365.

[12] M. Mirzaei, H. Eshtiagh-Hosseini, N. Lotfian, A. Salimi, A. Bauzá, R. Van Deun, R. Decadt, M. Barceló-Oliver, A. Frontera, Dalton Trans. 43 (2014) 1906-1916.

[13] M. Tahmasebi, M. Mirzaei, H. Eshtiagh-Hosseini, J.T. Mague, A. Bauzá, A. Frontera, Acta Crystallographica Section C: Structural Chemistry, 75 (2019) 469-477.

[14] M. Bazargan, M. Mirzaei, A. Franconetti, A. Frontera, Dalton Trans. 48 (2019) 5476-5490.

[15] M. Samaniyan, M. Mirzaei, R. Khajavian, H. Eshtiagh-Hosseini, C. Streb, ACS catalysis, 9 (2019) 10174-10191.

[16] S.-T. Zheng, G.-Y. Yang, Chem. Soc. Rev. 41 (2012) 7623-7646.

[17] J. Feng, C. Gao, Y. Yin, Nanoscale, 10 (2018) 20492-20504.

[18] D.I. Enache, J.K. Edwards, P. Landon, B. Solsona-Espriu, A.F. Carley, A.A. Herzing, M. Watanabe, C.J. Kiely, D.W. Knight, G.J. Hutchings, Science, 311 (2006) 362-365.

[19] Y. Xing, J. Phys. Chem. B 108 (2004) 19255-19259.

[20] K. Maeda, K. Teramura, D. Lu, T. Takata, N. Saito, Y. Inoue, K. Domen, Nature, 440 (2006) 295-295.

[21] G.J. Hutchings, M. Haruta, Appl. Catal., A 291 (2005) 2-5.

[22] H. Lv, W. Guo, K. Wu, Z. Chen, J. Bacsa, D.G. Musaev, Y.V. Geletii, S.M. Lauinger, T. Lian, C.L. Hill, J. Am. Chem. Soc. 136 (2014) 14015-14018.

[23] B. Li, X. Yu, H. Pang, Q. Shen, Y. Hou, H. Ma, J. Xin, Chem. Commun. 56 (2020) 7199-7202.

[24] M.A. Fashapoyeh, M. Mirzaei, H. Eshtiagh-Hosseini, A. Rajagopal, M. Lechner, R. Liu, C. Streb, Chem. Commun. 54 (2018) 10427-10430.

[25] P. Putaj, F. Lefebvre, Coord. Chem. Rev. 255 (2011) 1642-1685.

[26] T. Kurata, A. Uehara, Y. Hayashi, K. Isobe, Inorg. Chem. 44 (2005) 2524-2530.

[27] S. Angus-Dunne, Robert C. Burns, Donald C. Craig, Geoffrey A. Lawrance, Z. Anorg. Allg. Chem. 636 (2010) 727-734.

[28] S.A. Adonin, N.V. Izarova, C. Besson, P.A. Abramov, B. Santiago-Schubel, P. Kogerler, V.P. Fedin, M.N. Sokolov, Chem Commun (Camb), 51 (2015) 1222-1225.

[29] A.A. Mukhacheva, P.A. Abramov, M.N. Sokolov, J. Struct. Chem. 60 (2019) 647-653.

[30] M. Sadakane, S. Moroi, Y. Iimuro, N. Izarova, U. Kortz, S. Hayakawa, K. Kato, S. Ogo, Y. Ide, W. Ueda, Chem. Asian J. 7 (2012) 1331-1339.

[31] C. Rong, M.T. Pope, J. Am. Chem. Soc. 114 (1992) 2932-2938.

[32] M. Sadakane, D. Tsukuma, M.H. Dickman, B.S. Bassil, U. Kortz, M. Capron, W. Ueda, Dalton Trans. (2007) 2833-2838.

[33] M. Sadakane, Y. Iimuro, D. Tsukuma, B.S. Bassil, M.H. Dickman, U. Kortz, Y. Zhang, S. Ye, W. Ueda, Dalton Trans. (2008) 6692-6698.

[34] M. Sadakane, N. Rinn, S. Moroi, H. Kitatomi, T. Ozeki, M. Kurasawa, M. Itakura, S. Hayakawa, K. Kato, M. Miyamoto, Z. Anorg. Allg. Chem. 637 (2011) 1467-1474.

[35] M. Sadakane, D. Tsukuma, M.H. Dickman, B. Bassil, U. Kortz, M. Higashijima, W. Ueda, Dalton Trans. (2006) 4271-4276.

[36] B. Zhu, Z.-L. Lang, N.-N. Ma, L.-K. Yan, Z.-M. Su, Phys. Chem. Chem. Phys. 16 (2014) 18017-18022.

[37] V. Artero, D. Laurencin, R. Villanneau, R. Thouvenot, P. Herson, P. Gouzerh, A. Proust, Inorg. Chem. 44 (2005) 2826-2835.

[38] A. Bagno, M. Bonchio, A. Sartorel, G. Scorrano, Eur. J. Inorg. Chem. 2000 (2000) 17-20.

[39] M. Murakami, D. Hong, T. Suenobu, S. Yamaguchi, T. Ogura, S. Fukuzumi, J. Am. Chem. Soc. 133 (2011) 11605-11613.

[40] A. Yokoyama, K. Ohkubo, T. Ishizuka, T. Kojima, S. Fukuzumi, Dalton Trans. 41 (2012) 10006-10013.

[41] C.-G. Liu, X.-H. Guan, Mol. Phys. 111 (2013) 3733-3740.

[42] C. Besson, Y.V. Geletii, F.o. Villain, R. Villanneau, C.L. Hill, A. Proust, Inorg. Chem. 48 (2009) 9436-9443.

[43] V. Lahootun, C. Besson, R. Villanneau, F. Villain, L.-M. Chamoreau, K. Boubekeur, S. Blanchard, R. Thouvenot, A. Proust, J. Am. Chem. Soc. 129 (2007) 7127-7135.

[44] C. Besson, D.G. Musaev, V. Lahootun, R. Cao, L.M. Chamoreau, R. Villanneau, F. Villain, R. Thouvenot, Y.V. Geletii, C.L. Hill, Chem.: Eur. J. 15 (2009) 10233-10243.

[45] M.N. Sokolov, S.A. Adonin, D.A. Mainichev, P.L. Sinkevich, C. Vicent, N.B. Kompankov, A.L. Gushchin, V. Nadolinny, V.P. Fedin, Inorg. Chem. 52 (2013) 9675-9682.

[46] C.-G. Liu, S. Liu, T. Zheng, Inorg. Chem. 54 (2015) 7929-7935.

[47] D. Laurencin, E. Garcia Fidalgo, R. Villanneau, F. Villain, P. Herson, J. Pacifico, H. Stoeckli-Evans, M. Bénard, M.M. Rohmer, G. Süss-Fink, Chem.: Eur. J. 10 (2004) 208-217.

[48] V. Artero, A. Proust, P. Herson, F. Villain, C. Cartier dit Moulin, P. Gouzerh, J. Am. Chem. Soc. 125 (2003) 11156-11157.

[49] L.-H. Bi, E.V. Chubarova, N.H. Nsouli, M.H. Dickman, U. Kortz, B. Keita, L. Nadjo, Inorg. Chem. 45 (2006) 8575-8583.

[50] L.-H. Bi, U. Kortz, M.H. Dickman, B. Keita, L. Nadjo, Inorg. Chem. 44 (2005) 7485-7493.

[51] L.-H. Bi, G. Al-Kadamany, E.V. Chubarova, M.H. Dickman, L. Chen, D.S. Gopala, R.M. Richards, B. Keita, L. Nadjo, H. Jaensch, Inorg. Chem. 48 (2009) 10068-10077.

[52] D.-M. Zheng, R.-Q. Wang, Y. Du, G.-F. Hou, L.-X. Wu, L.-H. Bi, New J. Chem. 40 (2016) 8829-8836.

[53] R.-Q. Meng, L. Suo, G.-F. Hou, J. Liang, L.-H. Bi, H.-L. Li, L.-X. Wu, CrystEngComm, 15 (2013) 5867-5876.

[54] A. Sartorel, M. Carraro, G. Scorrano, R.D. Zorzi, S. Geremia, N.D. McDaniel, S. Bernhard, M. Bonchio, J. Am. Chem. Soc. 130 (2008) 5006-5007.

[55] Y.V. Geletii, B. Botar, P. Kögerler, D.A. Hillesheim, D.G. Musaev, C.L. Hill, Angew. Chem. Int. Ed. 47 (2008) 3896-3899.

[56] S. Yamaguchi, K. Uehara, K. Kamata, K. Yamaguchi, N. Mizuno, Chem. lett. 37 (2008) 328-329.

[57] A. Sartorel, P. Miró, E. Salvadori, S. Romain, M. Carraro, G. Scorrano, M.D. Valentin, A. Llobet, C. Bo, M. Bonchio, J. Am. Chem. Soc. 131 (2009) 16051-16053.

[58] Q. Han, Y. Ding, Dalton Trans. 47 (2018) 8180-8188.

[59] Y.V. Geletii, Z. Huang, Y. Hou, D.G. Musaev, T. Lian, C.L. Hill, J. Am. Chem. Soc. 131 (2009) 7522-7523.

[60] M. Orlandi, R. Argazzi, A. Sartorel, M. Carraro, G. Scorrano, M. Bonchio, F. Scandola, Chem. Commun. 46 (2010) 3152-3154.

[61] F. Puntoriero, G. La Ganga, A. Sartorel, M. Carraro, G. Scorrano, M. Bonchio, S. Campagna, Chem. Commun. 46 (2010) 4725-4727.

[62] T. Ishizuka, S. Ohkawa, H. Ochiai, M. Hashimoto, K. Ohkubo, H. Kotani, M. Sadakane, S. Fukuzumi, T. Kojima, Green chem. 20 (2018) 1975-1980.

[63] P.-E. Car, M. Guttentag, K.K. Baldridge, R. Alberto, G.R. Patzke, Green Chem. 14 (2012) 1680-1688.

[64] A. Sartorel, M. Truccolo, S. Berardi, M. Gardan, M. Carraro, F.M. Toma, G. Scorrano, M. Prato, M. Bonchio, Chem. Commun. 47 (2011) 1716-1718.

[65] H. Ma, S. Shi, Z. Zhang, H. Pang, Y. Zhang, J. Electroanal. Chem. 648 (2010) 128-133.

[66] N. Anwar, A. Sartorel, M. Yaqub, K. Wearen, F. Laffir, G. Armstrong, C. Dickinson, M. Bonchio, T. McCormac, ACS applied materials & interfaces, 6 (2014) 8022-8031.

[67] R.-Q. Wang, L. Suo, D.-M. Zheng, Y. Du, L.-X. Wu, L.-H. Bi, Inorg. Chim. Acta, 443 (2016) 218-223.

[68] C. Besson, Z. Huang, Y.V. Geletii, S. Lense, K.I. Hardcastle, D.G. Musaev, T. Lian, A. Proust, C.L. Hill, Chem. Commun. 46 (2010) 2784-2786.

[69] Y.V. Geletii, C. Besson, Y. Hou, Q. Yin, D.G. Musaev, D. Quiñonero, R. Cao, K.I. Hardcastle, A. Proust, P. Kögerler, J. Am. Chem. Soc. 131 (2009) 17360-17370.

[70] D. Quiñonero, A.L. Kaledin, A.E. Kuznetsov, Y.V. Geletii, C. Besson, C.L. Hill, D.G. Musaev, J. Phys. Chem. A 114 (2009) 535-542.

[71] S. Piccinin, S. Fabris, Phys. Chem. Chem. Phys. 13 (2011) 7666-7674.

[72] Z.-L. Lang, G.-C. Yang, N.-N. Ma, S.-Z. Wen, L.-K. Yan, W. Guan, Z.-M. Su, Dalton Trans. 42 (2013) 10617-10625.

[73] Y. Gao, L.-K. Yan, W. Guan, Z.-M. Su, Inorg. Chem. Front. 6 (2019) 969-974.

[74] P. Gobbo, L. Tian, B.V.V.S. Pavan Kumar, S. Turvey, M. Cattelan, A.J. Patil, M. Carraro, M. Bonchio, S. Mann, Nat. Commun. 11 (2020).

[75] A.R. Howells, A. Sankarraj, C. Shannon, J. Am. Chem. Soc. 126 (2004) 12258-12259.

[76] S. Ogo, N. Shimizu, K. Nishiki, N. Yasuda, T. Mizuta, T. Sano, M. Sadakane, Inorg. Chem. 53 (2014) 3526-3539.

[77] K. Nishiki, N. Umehara, Y. Kadota, X. López, J.M. Poblet, C.A. Mezui, A.-L. Teillout, I.M. Mbomekalle, P. de Oliveira, M. Miyamoto, Dalton Trans. 45 (2016) 3715-3726.

[78] K. Nomiya, H. Torii, K. Nomura, Y. Sato, J. Chem. Soc., Dalton Trans. (2001) 1506-1512.

[79] W.J. Randall, T.J. Weakley, R.G. Finke, Inorg. Chem. 32 (1993) 1068-1071.

[80] S.-F. Jia, X.-L. Hao, Y.-Z. Wen, Y. Zhang, J. Coord. Chem. 72 (2019) 633-644.

[81] A. Modvig, C. Kumpidet, A. Riisager, J. Albert, Materials, 12 (2019) 2175.

[82] R. Wan, H. Li, X. Ma, Z. Liu, V. Singh, P. Ma, C. Zhang, J. Niu, J. Wang, Dalton Trans. 48 (2019) 10327-10336.

[83] M. Han, Y. Niu, R. Wan, Q. Xu, J. Lu, P. Ma, C. Zhang, J. Niu, J. Wang, Chem.: Eur. J. 24 (2018) 11059-11066.

[84] R. Wan, Q. Xu, M. Han, P. Ma, C. Zhang, J. Niu, J. Wang, Materials, 11 (2018) 178.

[85] G. Marcu, I. Ciogolas, Rev. Roum. Chim. 24 (1979) 1049-1052.

[86] A.A. Mukhacheva, V.V. Volchek, P.A. Abramov, M.N. Sokolov, Inorg. Chem. Commun. 89 (2018) 10-12.

[87] N.V. Izarova, M.T. Pope, U. Kortz, Angew. Chem. Int. Ed. 51 (2012) 9492-9510.

[88] N.N. Sveshnikov, M.H. Dickman, M.T. Pope, Inorg. Chim. Acta, 359 (2006) 2721-2727.

[89] J.-S. Li, X.-J. Sang, W.-L. Chen, L.-C. Zhang, Z.-M. Su, C. Qin, E.-B. Wang, Inorg. Chem. Commun. 38 (2013) 78-82.

[90] M.N. Sokolov, S.A. Adonin, P.A. Abramov, D.A. Mainichev, N.F. Zakharchuk, V.P. Fedin, Chem. Commun. 48 (2012) 6666-6668.

[91] M.N. Sokolov, S.A. Adonin, P.L. Sinkevich, C. Vicent, D.A. Mainichev, V.P. Fedin, Dalton Trans. 41 (2012) 9889-9892.

[92] M.N. Sokolov, S.A. Adonin, P.L. Sinkevich, C. Vicent, D.A. Mainichev, V.P. Fedin, Z. Anorg. Allg. Chem. 640 (2014) 122-127.

[93] J.-H. Son, W.H. Casey, Dalton Trans. 44 (2015) 20330-20333.

[94] P. Yang, U. Kortz, Acc. Chem. Res. 51 (2018) 1599-1608.

[95] V. Kogan, Z. Aizenshtat, R. Popovitz-Biro, R. Neumann, Org. lett. 4 (2002) 3529-3532.

[96] S.J. Angus-Dunne, R.C. Burns, D.C. Craig, G.A. Lawrance, J. Chem. Soc., Chem. Commun. (1994) 523-524.

[97] N. Kuznetsova, L. Detusheva, L. Kuznetsova, M. Fedotov, V. Likholobov, J. Mol. Catal. Chem. 114 (1996) 131-139.

[98] N. Kuznetsova, L. Kuznetsova, Kinet. Catal. 50 (2009) 1-10.

[99] A.J. Stapleton, M.E. Sloan, N.J. Napper, R.C. Burns, Dalton Trans. (2009) 9603-9615.

[100] L. Kuznetsova, N. Kuznetsova, L. Detusheva, M. Fedotov, V. Likholobov, J. Mol. Catal. Chem. 158 (2000) 429-433.

[101] L. Detusheva, L. Kuznetsova, N. Kuznetsova, L. Dovlitova, A. Vlasov, V. Likholobov, Russ. J. Inorg. Chem. 53 (2008) 690.

[102] L.H. Bi, U. Kortz, B. Keita, L. Nadjo, L. Daniels, Eur. J. Inorg. Chem. 2005 (2005) 3034-3041.

[103] Z. Lin, N.V. Izarova, F.T. Mehari, U. Kortz, Z. Anorg. Allg. Chem. 644 (2018) 1379-1382.

[104] L.-H. Bi, U. Kortz, B. Keita, L. Nadjo, H. Borrmann, Inorg. Chem. 43 (2004) 8367-8372.

[105] L.-H. Bi, M.H. Dickman, U. Kortz, CrystEngComm, 11 (2009) 965-966.

[106] T. Hirano, K. Uehara, K. Kamata, N. Mizuno, J. Am. Chem. Soc. 134 (2012) 6425-6433.

[107] R. Villanneau, S. Renaudineau, P. Herson, K. Boubekeur, R. Thouvenot, A. Proust, Eur. J. Inorg. Chem. 2009 (2009) 479-488.

[108] N.V. Izarova, A. Banerjee, U. Kortz, Inorg. Chem. 50 (2011) 10379-10386.

[109] P. He, B. Xu, X. Xu, L. Song, X. Wang, Chem. sci. 7 (2016) 1011-1015.

[110] N.V. Izarova, R.I. Maksimovskaya, S. Willbold, P. Kögerler, Inorg. Chem. 53 (2014) 11778-11784.

[111] N.V. Izarova, B. Santiago-Schuebel, S. Willbold, V. Hess, P. Koegerler, Chem.: Eur. J. 22 (2016) 16052-16056.
[112] R. Villanneau, A. Proust, F. Robert, Chem. Commun. (1998) 1491-1492.
[113] H.I. Nogueira, F.A.A. Paz, P.A. Teixeira, J. Klinowski, Chem. Commun. (2006) 2953-2955.
[114] Y. Cui, L. Shi, Y. Yang, W. You, L. Zhang, Z. Zhu, M. Liu, L. Sun, Dalton Trans. 43 (2014) 17406-17415.
[115] J. Li, L. Wang, W. You, M. Liu, L. Zhang, X. Sang, Chinese J. Catal. 39 (2018) 534-541.
[116] J.C. Ye, J.J. Chen, R.M. Yuan, D.R. Deng, M.S. Zheng, L. Cronin, Q.F. Dong, J. Am. Chem. Soc. 140 (2018) 3134-3138.
[117] F. Gruber, M. Jansen, Angew. Chem. Int. Ed. 49 (2010) 4924-4926.
[118] Y. Kikukawa, Y. Kuroda, K. Yamaguchi, N. Mizuno, Angew. Chem. Int. Ed. 51 (2012) 2434-2437.
[119] Y. Kikukawa, Y. Kuroda, K. Suzuki, M. Hibino, K. Yamaguchi, N. Mizuno, Chem. Commun. 49 (2013) 376-378.
[120] Z.-y. Shi, J. Peng, Y.-g. Li, Z.-y. Zhang, X. Yu, K. Alimaje, X. Wang, CrystEngComm, 15 (2013) 7583.
[121] Z.-G. Jiang, K. Shi, Y.-M. Lin, Q.-M. Wang, Chem. Commun. 50 (2014) 2353-2355.
[122] C.-Y. Song, D.-F. Chai, R.-R. Zhang, H. Liu, Y.-F. Qiu, H.-D. Guo, G.-G. Gao, Dalton Trans. 44 (2015) 3997-4002.
[123] S.S. Zhang, H.F. Su, Z. Wang, X.P. Wang, W.X. Chen, Q.Q. Zhao, C.H. Tung, D. Sun, L.S. Zheng, Chem.: Eur. J. 24 (2018) 1998-2003.
[124] C. Zhan, J.M. Cameron, J. Gao, J.W. Purcell, D.L. Long, L. Cronin, Angew. Chem. Int. Ed. 53 (2014) 10362-10366.
[125] P. Yang, Y. Xiang, Z. Lin, Z. Lang, P. Jiménez-Lozano, J.J. Carbó, J.M. Poblet, L. Fan, C. Hu, U. Kortz, Angew. Chem. Int. Ed. 55 (2016) 15766-15770.
[126] S. Romo, N.S. Antonova, J.J. Carbó, J.M. Poblet, Dalton Trans. (2008) 5166-5172.
[127] H. Kwen, S. Tomlinson, E.A. Maatta, C. Dablemont, R. Thouvenot, A. Proust, P. Gouzerh, Chem. Commun. (2002) 2970-2971.
[128] L.K. Yan, Z. Dou, W. Guan, S.Q. Shi, Z.M. Su, Eur. J. Inorg. Chem. 2006 (2006) 5126-5129.
[129] D. Laurencin, R. Villanneau, H. Gérard, A. Proust, J. Phys. Chem. A 110 (2006) 6345-6355.
[130] C. Dablemont, C.G. Hamaker, R. Thouvenot, Z. Sojka, M. Che, E.A. Maatta, A. Proust, Chem.: Eur. J. 12 (2006) 9150-9160.
[131] W. Sun, H. Liu, J. Kong, G. Xie, J. Deng, J. Electroanal. Chem. 437 (1997) 67-76.
[132] R. Cao, H. Ma, Y.V. Geletii, K.I. Hardcastle, C.L. Hill, Inorg Chem, 48 (2009) 5596-5598.

[133] J. Zhang, S. Chang, B.H. Suryanto, C. Gong, X. Zeng, C. Zhao, Q. Zeng, J. Xie, Inorg. Chem. 55 (2016) 5585-5591.

[134] M.N. Sokolov, S.A. Adonin, D.A. Mainichev, C. Vicent, N.F. Zakharchuk, A.M. Danilenko, V.P. Fedin, Chem. Commun. 47 (2011) 7833-7835.

[135] M.N. Sokolov, S.A. Adonin, P.L. Sinkevich, C. Vicent, D.A. Mainichev, V.P. Fedin, Dalton Trans, 41 (2012) 9889-9892.

[136] C.M. Tourné, G.F. Tourné, F. Zonnevijlle, Journal of the Chemical Society, Dalton Trans. (1991) 143-155.

[137] R. Neumann, A.M. Khenkin, Inorg. Chem. 34 (1995) 5753-5760.

[138] U. Lee, H.-C. Joo, K.-M. Park, T. Ozeki, Acta Cryst.C 59 (2003) m152-m155.

[139] T.M. Anderson, W.A. Neiwert, M.L. Kirk, P.M. Piccoli, A.J. Schultz, T.F. Koetzle, D.G. Musaev, K. Morokuma, R. Cao, C.L. Hill, Science, 306 (2004) 2074-2077.

[140] U. Lee, H.C. Joo, K.M. Park, S.S. Mal, U. Kortz, B. Keita, L. Nadjo, Angew. Chem. Int. Ed. 47 (2008) 793-796.

[141] N. Vankova, T. Heine, U. Kortz, Eur. J. Inorg. Chem. 2009 (2009) 5102-5108.

[142] M. Kato, C.N. Kato, Inorg. Chem. Commun. 14 (2011) 982-985.

[143] C.N. Kato, S. Suzuki, T. Mizuno, Y. Ihara, A. Kurihara, S. Nagatani, Catal. Today, 332 (2019) 2-10.

[144] C.N. Kato, Y. Morii, S. Hattori, R. Nakayama, Y. Makino, H. Uno, Dalton Trans. 41 (2012) 10021-10027.

[145] Y.-D. Cao, D. Yin, M.-L. Wang, T. Pang, Y. Lv, B. Liu, G.-G. Gao, L. Ma, H. Liu, Dalton Trans. 49 (2020) 2176-2183.

[146] C.N. Kato, S. Nagatani, T. Mizuno, Eur. J. Inorg. Chem. 2019 (2019) 517-522.

[147] S. Hattori, Y. Ihara, C.N. Kato, Catal. Lett. 145 (2015) 1703-1709.

[148] M.N. Sokolov, S.A. Adonin, E.V. Peresypkina, V.P. Fedin, Dalton Trans. 41 (2012) 11978-11979.

[149] P. Abramov, C. Vicent, N. Kompankov, A. Gushchin, M. Sokolov, Chem. Commun. 51 (2015) 4021-4023.

[150] A.A. Shmakova, R.R. Shiriyazdanov, A.R. Karimova, N.B. Kompankov, P.A. Abramov, M.N. Sokolov, J. Clust. Sci. 29 (2018) 1201-1207.

[151] P. Klonowski, J.C. Goloboy, F.J. Uribe-Romo, F. Sun, L. Zhu, F. Gándara, C. Wills, R.J. Errington, O.M. Yaghi, W.G. Klemperer, Inorg. Chem. 53 (2014) 13239-13246.

[152] Z. Lin, N.V. Izarova, A. Kondinski, X. Xing, A. Haider, L. Fan, N. Vankova, T. Heine, B. Keita, J. Cao, Chem.: Eur. J. 22 (2016) 5514-5519.

[153] S. Dugar, N.V. Izarova, S.S. Mal, R. Fu, H.-C. Joo, U. Lee, N.S. Dalal, M.T. Pope, G.B. Jameson, U. Kortz, New J. Chem. 40 (2016) 923-927.

Dated: 11/14/ 2020

Editor

Journal of Inorganica Chimica Acta

Subject: <u>Conflict of Interest</u>

Dear Editor,

Hereby I declare that we have NO conflict of interest.

With best regards,

Masoud Mirzaei

Full Professor in Inorganic Chemistry

Department of Chemistry

Faculty of Science, Ferdowsi University of Mashhad

Mashhad, Iran

Tel: 00985138805554

Email: mirzaeesh@um.ac.ir

Morteza Tahmasebi was born in 1981 in Miandoab, Iran. He received his B.Sc. degree in 2005 from Kordestan University and his M.Sc. degree from IAU in 2011. In 2015, he started her Ph.D. in Ferdowsi University of Mashhad. His main interest is in bio-inorganic chemistry and chiral polyoxometalates. He is now pursuing his Ph.D. thesis under the supervision of Hossein Eshtiagh-Hosseini and Masoud Mirzaei considering synthesis of inorganic–organic hybrid based polyoxometalates and biomolecules in order to investigate intermolecular interactions within their crystalline networks.

Prof. Masoud Mirzaei was born in 1980 in Tehran, Iran. He obtained his PhD from Ferdowsi University of Mashhad (FUM) in 2010 and he is currently a full professor in Inorganic Chemistry at FUM. His research interests focus on synthesis and characterization of crystalline polyoxometalate-based frameworks as adsorbents and porous coordination polymers. These promising materials have a wide variety of applications in green chemistry and are used widely in various fields including gas storage, selective adsorption, and catalysis. In a recent published in Chemical Communications, he succeeded in demonstrating the application of these compounds in hydrogen evolution reactivity (HER) under photochemical and electrochemical conditions. He has published more than 170 ISI cited papers, reviews and one book chapter in LAP, so far. He has served as a reviewer for scientific journals from all continents, and has reviewed many manuscripts.

Prof. Hossein Eshtiagh-Hosseini was born in 1947 in Tabriz, Iran. He received his B.Sc. degree from Tabriz University in 1969 and his M.Sc., Ph.D., and postdoc degrees from the University of Sussex, England, in 1973, 1977, and 1979. He started his career as an assistant professor at FUM in 1979 and was promoted to associate professor in 2008 and full professor in 2012. His research interests focus on inorganic–organic hybrids based on polyoxometalates, coordination chemistry, and organometallic. He has published more than 130 papers, reviews and one book chapter in LAP so far.

Prof. A. Frontera received his PhD from the Universitat de les Illes Balears (Spain) in 1994. During this period, he combined theory and experiment to propose a plausible mechanism for the direct lithiation of polyphenolic compounds. Moreover, he studied the mechanism of diotropic reactions. After two years of postdoctoral research in the laboratory of Prof. W. L. Jorgensen (Yale University, USA), 1995–1996, devoted to the OPLS force field parameterization of carbohydrates, he came back to Spain as a research scientist at the Universitat de les Illes Balears, where he is currently a professor working on noncovalent interactions.